
Dynamical Mean-Field Theory

Dieter Vollhardt¹, Krzysztof Byczuk², and Marcus Kollar¹

¹ Theoretical Physics III, Center for Electronic Correlations and Magnetism,
Institute of Physics, University of Augsburg, 86135 Augsburg, Germany

² Institute of Theoretical Physics, Faculty of Physics, University of Warsaw, ul.
Hoża 69, 00-681 Warszawa, Poland

Abstract. The dynamical mean-field theory (DMFT) is a widely applicable approximation scheme for the investigation of correlated quantum many-particle systems on a lattice, e.g., electrons in solids and cold atoms in optical lattices. In particular, the combination of the DMFT with conventional methods for the calculation of electronic band structures has led to a powerful numerical approach which allows one to explore the properties of correlated materials. In this introductory article we discuss the foundations of the DMFT, derive the underlying self-consistency equations, and present several applications which have provided important insights into the properties of correlated matter.

1.1 Motivation

1.1.1 Electronic Correlations

Already in 1937, at the outset of modern solid state physics, de Boer and Verwey [1] drew attention to the surprising properties of materials with incompletely filled $3d$ -bands. This observation prompted Mott and Peierls [2] to discuss the interaction between the electrons. Ever since transition metal oxides (TMOs) were investigated intensively [3]. It is now well-known that in many materials with partially filled electron shells, such as the $3d$ transition metals V and Ni and their oxides, or $4f$ rare-earth metals such as Ce, electrons occupy narrow orbitals. The spatial confinement enhances the effect of the Coulomb interaction between the electrons, making them “strongly correlated”. Correlation effects can lead to profound quantitative and qualitative changes of the physical properties of electronic systems as compared to non-interacting particles. In particular, they often respond very strongly to changes in external parameters. This is expressed by large renormalizations of the response functions of the system, e.g., of the spin susceptibility and the charge compressibility. In particular, the interplay between the spin, charge and orbital degrees of freedom of the correlated d and f electrons and with the lattice degrees of freedom leads to an amazing multitude of ordering phenomena and other fascinating properties, including high temperature superconductivity, colossal magnetoresistance and Mott metal-insulator transitions [3].

1.1.2 The Hubbard Model

The simplest microscopic model describing interacting electrons in a solid is the one-band, spin-1/2 Hubbard model [4–6] where the interaction between the electrons is assumed to be so strongly screened that it is purely local. More generally the Hubbard model applies to lattice fermions with a point interaction, such as ultra-cold fermionic atoms in optical lattices where the interaction is indeed extremely short ranged. The Hamiltonian consists of two terms, the kinetic energy \hat{H}_0 and the interaction energy \hat{H}_I (here and in the following operators are denoted by a hat):

$$\hat{H} = \hat{H}_0 + \hat{H}_I \quad (1.1a)$$

$$\hat{H}_0 = \sum_{i,j} \sum_{\sigma} t_{ij} \hat{c}_{i\sigma}^{\dagger} \hat{c}_{j\sigma} = \sum_{\mathbf{k},\sigma} \epsilon_{\mathbf{k}} \hat{n}_{\mathbf{k}\sigma} \quad (1.1b)$$

$$\hat{H}_I = U \sum_i \hat{n}_{i\uparrow} \hat{n}_{i\downarrow}, \quad (1.1c)$$

where $\hat{c}_{i\sigma}^{\dagger}$ ($\hat{c}_{i\sigma}$) are creation (annihilation) operators of fermions with spin σ at site \mathbf{R}_i (for simplicity denoted by i), and $\hat{n}_{i\sigma} = \hat{c}_{i\sigma}^{\dagger} \hat{c}_{i\sigma}$. The Fourier transform of the kinetic energy in (1.1b), where t_{ij} is the amplitude for hopping between sites i and j , involves the dispersion $\epsilon_{\mathbf{k}}$ and the momentum distribution operator $\hat{n}_{\mathbf{k}\sigma}$. This model provides the basis for most of the theoretical research on correlated electrons during the last decades.

The Hubbard model describes an interacting many-body system which cannot be solved analytically, except in dimension $d = 1$ for nearest-neighbor hopping [7]. In the absence of exact solutions there is clearly a great need for reliable, controlled approximation schemes for this model. However, such approximations are not easy to construct as the following observation shows. When viewed as a function of time a given site of the lattice will sometimes be empty, singly occupied or doubly occupied. For strong repulsion U double occupations are energetically very unfavorable and are therefore strongly suppressed, implying $\langle \hat{n}_{i\uparrow} \hat{n}_{i\downarrow} \rangle \neq \langle \hat{n}_{i\uparrow} \rangle \langle \hat{n}_{i\downarrow} \rangle$. Therefore approximation schemes based on the factorization of the interaction term, e.g., Hartree-Fock-type mean-field theories, are generally insufficient to explain the physics of electrons in their paramagnetic phase beyond the limit of weak interactions. This is due to the fact that in such approximations the interaction is described only as an average, static potential, whereby correlations, i.e., dynamical many-body effects due to the interaction of individual electrons, are excluded from the beginning. Hence correlation phenomena such as the Mott-Hubbard metal-insulator transition cannot be described by such approximations. This clearly shows the need for comprehensive approximation schemes, which are applicable for all values of the input parameters, e.g., coupling parameters and temperature, diagrammatically controlled, and thermodynamically consistent [8].

1.1.3 Construction of Comprehensive Mean-Field Theories for Many-Particle Models

There exists a well-established branch of approximation techniques which makes use of the simplifications that occur when some parameter is taken to be large (in fact, infinite), e.g., the length of the spins S , the spin degeneracy

N , the spatial dimension d , or the coordination number Z , i.e., the number of nearest neighbors of a lattice site.³ Investigations in this limit, supplemented if possible by an expansion in the inverse of the large parameter, often provide valuable insights into the fundamental properties of a system even when the inverse parameter is not very small.

One of the best-known mean-field theories in many-body physics is the Weiss molecular-field theory for the Ising model [10]. It is a prototypical *single-site mean-field theory* which becomes exact for infinite-range interaction, as well as in the limit of the coordination number $Z \rightarrow \infty$ or the dimension $d \rightarrow \infty$. In the latter case $1/Z$ or $1/d$ is a small parameter which can be used to improve the mean-field theory systematically. This mean-field theory is comprehensive in the sense discussed above. Namely, it contains no unphysical singularities, is applicable for all values of the input parameters, i.e., the coupling parameter, magnetic field, and temperature, and is diagrammatically controlled [11].

Itinerant quantum mechanical models such as the Hubbard model and its generalizations are much more complicated than classical, Ising-type models. Generally there do not even exist semiclassical approximations for such models that might serve as a starting point for further investigations. Under such circumstances the construction of a mean-field theory with the comprehensive properties of the Weiss molecular field theory for the Ising model will necessarily be much more complicated, too. Here the limit of high spatial dimensions d or coordination number Z has again been extremely useful since it provides the basis for the construction of a comprehensive *dynamical* mean-field theory (DMFT) for lattice fermions.

In this article we will first discuss (sec. 1.2) the limit of high spatial dimensions d for lattice fermions, the scaling of the hopping amplitude which is necessary to obtain a meaningful limit $d \rightarrow \infty$ as well as the simplifications of the many-body perturbation theory occurring in this limit. In sec. 1.3 the self-consistency equations obtained in the limit $d \rightarrow \infty$ are derived which provide the basis for the DMFT for correlated lattice fermions. An example for the many insights gained by the DMFT is the Mott-Hubbard metal-insulator transition discussed in sec. 1.4. The application of the DMFT to real correlated materials is described in sec. 1.5. Brief introductions to the DMFT for correlated systems in the presence of disorder (sec. 1.6), correlated bosons in optical lattices (sec. 1.7), and systems in non-equilibrium (sec. 1.8) are also given. In sec. 1.9 a summary and outlook is presented.

³ The coordination number Z is determined by the dimension d and the lattice structure. Already in $d = 3$ the coordination number can be quite large, e.g., $Z = 6$ for a simple cubic lattice, $Z = 8$ for a bcc lattice and $Z = 12$ for an fcc-lattice, making its inverse, $1/Z$, rather small. It is then natural to consider the limit $Z \rightarrow \infty$ to simplify the problem. For a hypercubic lattice, obtained by generalizing the simple cubic lattice in $d = 3$ to arbitrary dimensions, one has $Z = 2d$. The limit $d \rightarrow \infty$ is then equivalent to $Z \rightarrow \infty$. Several standard approximation schemes which are commonly used to explain experimental results in dimension $d = 3$ are exact only in $d, Z = \infty$ [9].

1.2 Lattice Fermions in the Limit of High Dimensions

1.2.1 Scaling of the Hopping Amplitude

We consider the kinetic energy term (1.1a) since the interaction term is purely local and is thereby completely independent of the lattice structure and the dimension. For hopping between nearest-neighbor (NN) sites i and j with amplitude $t_{ij} \equiv -t$ on a d -dimensional hypercubic lattice with lattice spacing a , the dispersion $\epsilon_{\mathbf{k}}$ is given by

$$\epsilon_{\mathbf{k}} = -2t \sum_{n=1}^d \cos(k_n a). \quad (1.2)$$

The density of states (DOS) corresponding to $\epsilon_{\mathbf{k}}$ is

$$N_d(\omega) = \sum_{\mathbf{k}} \delta(\hbar\omega - \epsilon_{\mathbf{k}}), \quad (1.3)$$

which is the probability density for finding⁴ $\omega = \epsilon_{\mathbf{k}}$ for a random choice of $\mathbf{k} = (k_1, \dots, k_d)$. If the k_i are chosen randomly, $\epsilon_{\mathbf{k}}$ in (1.2) is the sum of (independent) random numbers $-2t \cos k_i$. The central limit theorem then implies [12] that in the limit $d \rightarrow \infty$ the DOS is given by a Gaussian

$$N_d(\omega) \xrightarrow{d \rightarrow \infty} \frac{1}{2t\sqrt{\pi d}} \exp \left[- \left(\frac{\omega}{2t\sqrt{d}} \right)^2 \right]. \quad (1.4)$$

Unless t is scaled properly with d this DOS will become arbitrarily broad and featureless for $d \rightarrow \infty$. Clearly only the scaling

$$t \rightarrow \frac{t^*}{\sqrt{d}}, \quad t^* = \text{const.}, \quad (1.5)$$

(“quantum scaling”) yields a non-trivial limit $d \rightarrow \infty$ for the DOS [13, 12].

The interaction term in (1.1) is seen to be purely local and independent of the surrounding; hence it is independent of the spatial dimension of the system. Consequently, the on-site interaction U need not be scaled. So we see that the scaled Hubbard Hamiltonian

$$\hat{H} = -\frac{t^*}{\sqrt{Z}} \sum_{\langle i, j \rangle} \sum_{\sigma} \hat{c}_{i\sigma}^+ \hat{c}_{j\sigma} + U \sum_i \hat{n}_{i\uparrow} \hat{n}_{i\downarrow} \quad (1.6)$$

has a nontrivial $Z \rightarrow \infty$ limit, where both terms, the kinetic energy and the interaction, are of the same order of magnitude and are thereby able to compete; here $\langle i, j \rangle$ denotes NN sites i and j . It is this competition between the two terms which leads to interesting many-body physics. Mathematically this is expressed by the fact that the generic matrix elements of the commutator between the kinetic and the interaction part of the Hamiltonian do not vanish in the $d \rightarrow \infty$ limit.

The quantum scaling (1.5) was determined within a \mathbf{k} -space formulation, but it can also be derived within a position-space formulation as will be discussed next.

⁴ In the following we set the Planck constant \hbar , the Boltzmann constant k_B , and the lattice constant a equal to unity.

1.2.2 Simplifications of the Many-Body Perturbation Theory

The most important consequence of the scaling (1.5) is the fact that it leads to significant simplifications in the investigation of Hubbard-type lattice models [12, 14–19]. To understand this point better we take a look at the perturbation theory in terms of U . At $T = 0$ and $U = 0$ the kinetic energy of the electrons is given by

$$E_{\text{kin}}^0 = -t \sum_{\langle i,j \rangle} \sum_{\sigma} g_{ij,\sigma}^0. \quad (1.7)$$

Here $g_{ij,\sigma}^0 = \langle \hat{c}_{i\sigma}^{\dagger} \hat{c}_{j\sigma} \rangle_0$ is the one-particle density matrix which can be interpreted as the probability amplitude for hopping from site j to site i . The square of its absolute value is proportional to the probability for an electron to hop from j to i , i.e., $|g_{ij,\sigma}^0|^2 \sim 1/Z \sim 1/d$, since site j has $\mathcal{O}(d)$ NN sites i . The sum of $|g_{ij,\sigma}^0|^2$ over all NN sites i of j must then yield a Z or d independent constant. In the limit $d \rightarrow \infty$ we therefore find

$$g_{ij,\sigma}^0 \sim \mathcal{O}\left(\frac{1}{\sqrt{d}}\right). \quad (1.8)$$

Since the sum over NN sites in (1.7) is of $\mathcal{O}(d)$, the NN hopping amplitude t must obviously be scaled according to (1.5) for E_{kin}^0 to remain finite in the limit $d, Z \rightarrow \infty$. Hence, as expected, a real-space formulation yields the same results for the required scaling of the hopping amplitude.

The one-particle Green function $G_{ij,\sigma}^0(\omega)$ of the non-interacting system obeys the same scaling as $g_{ij,\sigma}^0$. This follows directly from its definition

$$G_{ij,\sigma}^0(t) \equiv -\langle T \hat{c}_{i\sigma}(t) \hat{c}_{j\sigma}^{\dagger}(0) \rangle_0, \quad (1.9)$$

where T is the time ordering operator, and the time evolution of the operators is given by the Heisenberg representation. The one-particle density matrix is obtained as $g_{ij,\sigma}^0 = \lim_{t \rightarrow 0^-} G_{ij,\sigma}^0(t)$. If $g_{ij,\sigma}^0$ obeys (1.8) the one-particle Green function must follow the same scaling at all times since this property does not depend on the time evolution and the quantum mechanical representation. The Fourier transform $G_{ij,\sigma}^0(\omega)$ also preserves this property.

It is important to realize that, although $G_{ij,\sigma}^0 \sim 1/\sqrt{d}$ vanishes for $d \rightarrow \infty$, the particles are *not* localized, but are still mobile. Indeed, even in the limit $d \rightarrow \infty$ the off-diagonal elements of $G_{ij,\sigma}^0$ contribute, since a particle may hop to d nearest neighbors with reduced amplitude $t^*/\sqrt{2d}$. For general i, j one finds [20, 15]

$$G_{ij,\sigma}^0 \sim \mathcal{O}\left(1/d^{||\mathbf{R}_i - \mathbf{R}_j||/2}\right), \quad (1.10)$$

where $||\mathbf{R}|| = \sum_{n=1}^d |R_n|$ is the length of \mathbf{R} in the so-called ‘‘New York metric’’ (also called ‘‘taxi cab metric’’, since particles only hop along horizontal or vertical lines, never along a diagonal).

It is the property (1.10) which is the origin of all simplifications arising in the limit $d \rightarrow \infty$. In particular, it implies the collapse of all connected, irreducible perturbation theory diagrams in position space [12, 14, 15]. In general, any two vertices which are connected by more than two separate paths⁵ will collapse onto the same site. In particular, the external vertices of any

⁵ Here a ‘‘path’’ is any sequence of lines in a diagram; they are ‘‘separate’’ when they have no lines in common.

irreducible self-energy diagram are always connected by three separate paths and hence always collapse. As a consequence the full irreducible self-energy becomes a purely local quantity [12], but retains its dynamics [14]

$$\Sigma_{ij,\sigma}(\omega) \stackrel{d \rightarrow \infty}{\equiv} \Sigma_{ii,\sigma}(\omega) \delta_{ij}. \quad (1.11a)$$

In the paramagnetic phase we may write $\Sigma_{ii,\sigma}(\omega) \equiv \Sigma(\omega)$. The Fourier transform of $\Sigma_{ij,\sigma}$ is then momentum-independent

$$\Sigma_{\sigma}(\mathbf{k}, \omega) \stackrel{d \rightarrow \infty}{\equiv} \Sigma_{\sigma}(\omega). \quad (1.11b)$$

This leads to tremendous simplifications in all many-body calculations for the Hubbard model and related models. It should be noted that a \mathbf{k} -independence of Σ was sometimes *assumed* as a convenient approximation (“local approximation”) [21–23]. Here we identified the limit where this is indeed exact.

1.2.3 Interactions Beyond the On-Site Interaction

In the case of more general interactions than the Hubbard interaction, e.g., nearest-neighbor interactions such as

$$\hat{H}_{nn} = \sum_{\langle i,j \rangle} \sum_{\sigma\sigma'} V_{\sigma\sigma'} \hat{n}_{i\sigma} \hat{n}_{j\sigma'} \quad (1.12)$$

the interaction constant has to be scaled, too, in the limit $d \rightarrow \infty$. In the case of (1.12), which has the form of a classical interaction, the “classical” scaling

$$V_{\sigma\sigma'} \rightarrow \frac{V_{\sigma\sigma'}^*}{Z} \quad (1.13)$$

is required. Of course, the propagator still has the dependence (1.10).

Due to (1.13) all contributions, except for the Hartree term, are found to vanish in $d = \infty$ [14]. Hence nonlocal interactions only contribute via their Hartree contribution, which is purely static. This gives the Hubbard interaction a unique role: of all interactions for fermionic lattice models only the purely local Hubbard interaction remains dynamical in the limit $d \rightarrow \infty$ [14].

1.2.4 Single-Particle Propagator

Due to the \mathbf{k} -independence of the irreducible self-energy, (1.11b), the one-particle propagator of an interacting lattice fermion system is given by

$$G_{\mathbf{k},\sigma}(\omega) = \frac{1}{\omega - \epsilon_{\mathbf{k}} + \mu - \Sigma_{\sigma}(\omega)}. \quad (1.14)$$

Most importantly, the \mathbf{k} dependence of $G_{\mathbf{k}}(\omega)$ comes entirely from the energy dispersion $\epsilon_{\mathbf{k}}$ of the *non*-interacting particles. This means that for a homogeneous system with the propagator

$$G_{ij,\sigma}(\omega) = L^{-1} \sum_{\mathbf{k}} G_{\mathbf{k},\sigma}(\omega) e^{i\mathbf{k} \cdot (\mathbf{R}_i - \mathbf{R}_j)} \quad (1.15)$$

its local part, $G_{ii,\sigma}$, has the form [16]

$$G_{ii,\sigma}(\omega) = L^{-1} \sum_{\mathbf{k}} G_{\mathbf{k},\sigma}(\omega) = \int_{-\infty}^{\infty} dE \frac{N_{\infty}(E)}{\omega - E + \mu - \Sigma_{\sigma}(\omega)} \quad (1.16a)$$

$$\equiv G_{\sigma}(\omega). \quad (1.16b)$$

In the following we will limit our discussion to the paramagnetic phase and omit the spin index. The spectral function of the interacting system (often referred to as the “density of states” (DOS) as in the non-interacting case) is given by

$$A(\omega) = -\frac{1}{\pi} \text{Im}G(\omega + i0^+); \quad (1.16c)$$

for $U = 0$ one has $A(\omega) \equiv N(\omega)$. In the limit $d \rightarrow \infty$ two quantities then play the most important role: the local propagator $G(\omega)$ and the self-energy $\Sigma(\omega)$.

1.2.5 Consequences of the Momentum Independence of the Self-Energy

We now discuss some more consequences of the \mathbf{k} -independence of the self-energy as derived by Müller-Hartmann [16]. Let us consider the Hubbard model, or any one of its generalizations, in the paramagnetic phase, i.e., without a broken symmetry. At $T = 0$ the one-particle Green function (1.14) then reads

$$G_{\mathbf{k}}(\omega) = \frac{1}{\omega - \epsilon_{\mathbf{k}} + E_F - \Sigma(\omega)}. \quad (1.17)$$

In general, even when $\Sigma(\omega)$ is \mathbf{k} -dependent, the Fermi surface is defined by the $\omega = 0$ limit of the denominator of (1.17) as

$$\epsilon_{\mathbf{k}} + \Sigma_{\mathbf{k}}(0) = E_F. \quad (1.18a)$$

According to Luttinger and Ward [24] the volume within the Fermi surface is not changed by interactions, provided the effect of the latter can be treated in infinite-order perturbation theory (i.e., no broken symmetry). This is expressed by

$$n = \sum_{\mathbf{k}\sigma} \theta[E_F - \epsilon_{\mathbf{k}} - \Sigma_{\mathbf{k}}(0)], \quad (1.18b)$$

where n is the particle density and $\theta(x)$ is the step function. In general, the \mathbf{k} -dependence of $\Sigma_{\mathbf{k}}(0)$ in (1.18a) implies that, in spite of (1.18b), the shape of the Fermi surface of the interacting system will be quite different from that of the non-interacting system (except for the fully rotation invariant case $\epsilon_{\mathbf{k}} \sim k^2$). For lattice fermion models in $d < \infty$, with $\Sigma_{\mathbf{k}}(\omega) \equiv \Sigma(\omega)$, (1.18a) implies that the Fermi surface itself (and hence the volume enclosed) is not changed by interactions.⁶ The Fermi energy is simply shifted uniformly from its non-interacting value E_F^0 , i.e., $E_F = E_F^0 + \Sigma(0)$, to keep n in (1.18b) constant. From (1.16a) we thus conclude that the $\omega = 0$ value of the local propagator, $G(0)$, and hence of the spectral function, $A(0) = -\frac{1}{\pi} \text{Im}G(i0^+)$, is not changed by interactions. Renormalizations of $A(0)$ can only come from a \mathbf{k} -dependence of Σ , i. e., if $\partial\Sigma/\partial\mathbf{k} \neq 0$.

For $\omega \rightarrow 0$ the self-energy has the property

⁶ In $d = \infty$ limit the notion of a Fermi surface of a lattice system is complicated by the fact that the dispersion $\epsilon_{\mathbf{k}}$ is not a simple smooth function.

$$\text{Im } \Sigma(\omega) \propto \omega^2 \quad (1.18c)$$

which implies quasiparticle (Fermi liquid) behavior. The effective mass

$$\frac{m^*}{m} = 1 - \left. \frac{d\Sigma}{d\omega} \right|_{\omega=0} = 1 + \frac{1}{\pi} \int_{-\infty}^{\infty} d\omega \frac{\text{Im}\Sigma(\omega + i0^-)}{\omega^2} \geq 1 \quad (1.18d)$$

is seen to be enhanced. In particular, the momentum distribution

$$n_{\mathbf{k}} = \frac{1}{\pi} \int_{-\infty}^0 d\omega \text{Im}G_{\mathbf{k}}(\omega) \quad (1.19)$$

has a discontinuity at the Fermi surface, given by $n_{k_F^-} - n_{k_F^+} = (m^*/m)^{-1}$, where $k_F^\pm = k_F \pm 0^+$.

1.3 Dynamical Mean-Field Theory for Correlated Lattice Fermions

The limit of high spatial dimensions d or coordination number Z provides the basis for the construction of a comprehensive mean-field theory for lattice fermions which is diagrammatically controlled and whose free energy has no unphysical singularities. It starts from the scaled Hamiltonian (1.6) and makes use of the simplifications in the many-body perturbation theory discussed in sec. 1.2.2. There we found that the local propagator $G(\omega)$, i.e., the probability amplitude for an electron to return to a lattice site, and the local, but fully dynamical self-energy $\Sigma(\omega)$ are the most important quantities in such a theory. Since the self-energy is a dynamical variable (in contrast to the Hartree-Fock theory where it is merely an average, static potential) the resulting mean-field theory is also dynamical and can thus describe genuine correlation effects such as the Mott-Hubbard metal-insulator transition.

The self-consistency equations of this *dynamical mean-field theory* (DMFT) for correlated lattice fermions can be derived in different ways. All derivations make use of the fact that in the limit of high spatial dimensions Hubbard-type models, i.e., lattice models with a local interaction, reduce to a “dynamical single-site problem”, where the d -dimensional lattice model is effectively described by the dynamics of the correlated fermions on a single site embedded in a “bath” provided by the other particles. In particular, the derivation by Janiš [25, 26] is a generalization of the coherent potential approximation (CPA) for disordered systems⁷ to the Hubbard model. In the following we will present today’s standard derivation by Georges and Kotliar [31] which is based on the mapping of the lattice problem onto a self-consistent single-impurity Anderson model; this approach was also employed by Jarrell [32]. Although the DMFT equations derived within the CPA approach and the self-consistent single-impurity approach, respectively, are identical it is the latter formulation which was immediately adopted by the community since it makes contact with the theory of quantum impurities and Kondo problems; for a review see [33]. This is a well-understood branch of many-body physics [34] for whose solution efficient numerical codes had been developed already in the 1980’s, in particular by use of the quantum Monte-Carlo (QMC) method [35].

⁷ The CPA is the best single-site approximation for disordered, non-interacting lattice electrons [27–29]; it becomes exact in the limit $d, Z \rightarrow \infty$ [30, 8].

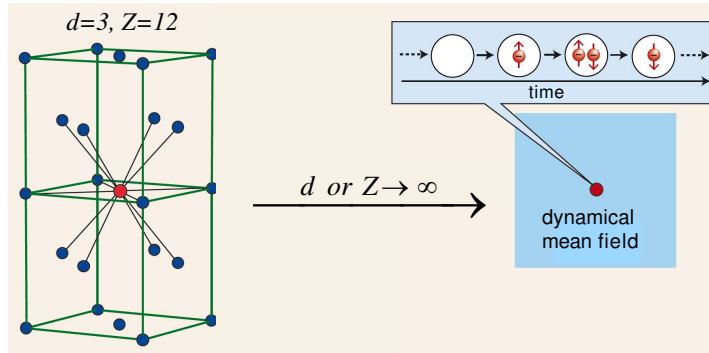


Fig. 1.1. Already in a $d = 3$ the coordination number Z can be quite large, as in the case of a face-centered cubic lattice with $Z = 12$. In the limit $d \rightarrow \infty$, i.e., $Z \rightarrow \infty$, the many-body lattice problem reduces to that of a single lattice site embedded in a dynamical mean field. As shown in the inset electrons can hop onto and off that site and interact as in the finite-dimensional Hubbard model. Therefore the DMFT describes the dynamics of the interacting electrons correctly.

1.3.1 Construction of the DMFT as a Self-Consistent Single-Impurity Anderson Model

Following the presentation of Georges, Kotliar, Krauth, and Rozenberg [33] the DMFT equations will now be derived using the so-called cavity method⁸. This derivation starts by removing one lattice site together with its bonds from the rest of the lattice. The remaining lattice, which now contains a cavity, is replaced by a particle bath which plays the role of the dynamical mean field (see Fig. 1.1). Now comes a physically motivated step: the bath is coupled, via a hybridization, to the cavity. The resulting problem then amounts to the solution of an effective single-impurity Anderson model where the degrees of freedom of the bath, represented by an appropriate hybridization function, have to be determined self-consistently.

To be specific, we consider the partition function in the grand canonical ensemble

$$\mathcal{Z} = \int \prod_{i\sigma} Dc_{i\sigma}^* Dc_{i\sigma} \exp[-S]. \quad (1.20)$$

The action S for the Hubbard model is given by

$$S = \int_0^\beta d\tau \left[\sum_{i\sigma} c_{i\sigma}^*(\tau) \left(\frac{\partial}{\partial \tau} - \mu \right) c_{i\sigma}(\tau) + \sum_{ij\sigma} t_{ij} c_{i\sigma}^*(\tau) c_{j\sigma}(\tau) + \sum_i U c_{i\uparrow}^*(\tau) c_{i\uparrow}(\tau) c_{i\downarrow}^*(\tau) c_{i\downarrow}(\tau) \right], \quad (1.21)$$

where we use Grassmann variables $c_{i\sigma}^*$, $c_{i\sigma}$. We split the action S into three parts

$$S = S_0 + \Delta S + S^{(0)}, \quad (1.22)$$

where S_0 is the part containing only variables on site 0

⁸ We note that the sign of the hopping amplitude t_{ij} used here (see the definition in (1.1b)) is opposite to that in ref. [33].

$$S_0 = \int_0^\beta d\tau \left[\sum_\sigma c_{0\sigma}^*(\tau) \left(\frac{\partial}{\partial \tau} - \mu \right) c_{0\sigma}(\tau) + U c_{0\uparrow}^*(\tau) c_{0\uparrow}(\tau) c_{0\downarrow}^*(\tau) c_{0\downarrow}(\tau) \right], \quad (1.23)$$

ΔS contains the hoppings between site 0 and other sites of the lattice $i \neq 0$

$$\Delta S = \int_0^\beta d\tau \sum_{i\sigma} [t_{i0} c_{i\sigma}^*(\tau) c_{0\sigma}(\tau) + t_{0i} c_{0\sigma}^*(\tau) c_{i\sigma}(\tau)], \quad (1.24)$$

and the rest, denoted by $S^{(0)}$, is the part of the action where the site 0 and its bonds are removed, i.e., for $i, j \neq 0$ one has

$$S^{(0)} = \int_0^\beta d\tau \left[\sum_{i \neq 0, \sigma} c_{i\sigma}^*(\tau) \left(\frac{\partial}{\partial \tau} - \mu \right) c_{i\sigma}(\tau) + \sum_{ij \neq 0, \sigma} t_{ij} c_{i\sigma}^*(\tau) c_{j\sigma}(\tau) + U \sum_{i \neq 0} c_{i\uparrow}^*(\tau) c_{i\uparrow}(\tau) c_{i\downarrow}^*(\tau) c_{i\downarrow}(\tau) \right]. \quad (1.25)$$

We now rewrite the partition function \mathcal{Z} as

$$\mathcal{Z} = \int \prod_\sigma Dc_{0\sigma}^* Dc_{0\sigma} \exp[-S_0] \times \int \prod_{i \neq 0, \sigma} Dc_{i\sigma}^* Dc_{i\sigma} \exp[-S^{(0)}] \exp[-\Delta S] \quad (1.26)$$

and use the ensemble average

$$\langle X \rangle_{(0)} \equiv \frac{1}{\mathcal{Z}^{(0)}} \int \prod_{i \neq 0, \sigma} Dc_{i\sigma}^* Dc_{i\sigma} X \exp[-S^{(0)}] \quad (1.27)$$

taken with respect to $S^{(0)}$ (the action where the site $i = 0$ is excluded), with $\mathcal{Z}^{(0)}$ being the corresponding partition function. Then the partition function reads

$$\mathcal{Z} = \mathcal{Z}^{(0)} \int \prod_\sigma Dc_{0\sigma}^* Dc_{0\sigma} \exp[-S_0] \langle \exp[-\Delta S] \rangle_{(0)}. \quad (1.28)$$

In the next step we expand the second exponent with respect to the action ΔS . A non-trivial limit $d \rightarrow \infty$ is obtained by scaling the hopping amplitudes t_{ij} as described in sec. 1.2.2. Consequently, in the $Z \rightarrow \infty$ limit only the contribution $G_{jk\sigma}^{(0)}$, where

$$G_{jk\sigma}^{(0)}(\tau_1 - \tau_2) = -\langle T_\tau c_{j\sigma}(\tau_1) c_{k\sigma}^*(\tau_2) \rangle_{(0)}, \quad (1.29)$$

or disconnected contributions made of products of $G_{jk\sigma}^{(0)}$'s remain. Applying the linked-cluster theorem and collecting only connected contributions in the exponential function one obtains the local action

$$\begin{aligned}
 S_{\text{loc}} = & \left[\int_0^\beta d\tau \sum_\sigma c_{0\sigma}^*(\tau) \left(\frac{\partial}{\partial \tau} - \mu \right) c_{0\sigma}(\tau) \right. \\
 & + U \int_0^\beta d\tau c_{0\uparrow}^*(\tau) c_{0\uparrow}(\tau) c_{0\downarrow}^*(\tau) c_{0\downarrow}(\tau) \\
 & \left. + \int_0^\beta d\tau_1 \int_0^\beta d\tau_2 \sum_\sigma \sum_{j,k \neq 0} t_{j0}^* t_{k0}^* G_{jk\sigma}^{(0)}(\tau_1 - \tau_2) c_{0\sigma}^*(\tau_1) c_{0\sigma}(\tau_2) \right], \quad (1.30)
 \end{aligned}$$

where the rescaled hoppings are denoted with a star. Introducing the hybridization function

$$\Delta_\sigma(\tau_1 - \tau_2) = - \sum_{i,j \neq 0} t_{i0}^* t_{j0}^* G_{ij\sigma}^{(0)}(\tau_1 - \tau_2), \quad (1.31)$$

and employing the free (“Weiss”) mean-field propagator \mathcal{G}_σ one can express the DMFT local action in the following form (here the site index $i = 0$ is omitted for simplicity)

$$\begin{aligned}
 S_{\text{loc}} = & - \int_0^\beta d\tau_1 \int_0^\beta d\tau_2 \sum_\sigma c_\sigma^*(\tau_1) \mathcal{G}_\sigma^{-1}(\tau_1 - \tau_2) c_\sigma(\tau_2) \\
 & + U \int_0^\beta d\tau c_\uparrow^*(\tau) c_\uparrow(\tau) c_\downarrow^*(\tau) c_\downarrow(\tau), \quad (1.32)
 \end{aligned}$$

where

$$\mathcal{G}_\sigma^{-1}(\tau_1 - \tau_2) = - \left(\frac{\partial}{\partial \tau_1} - \mu \right) \delta_{\tau_1 \tau_2} - \Delta_\sigma(\tau_1 - \tau_2). \quad (1.33)$$

Finally, we need the relation between the Green function $G_{ij\sigma}^{(0)}(\tau - \tau')$ where the site $i = 0$ is removed and the full lattice Green function, i.e.,

$$G_{ij\sigma}^{(0)} = G_{ij\sigma} - G_{i0\sigma} G_{00\sigma}^{-1} G_{0j\sigma}, \quad (1.34)$$

which holds for a general lattice.

In order to obtain the full solution of the lattice problem it is convenient to express the relation between the local Green function $G_{00\sigma} \equiv G_\sigma$ and the “Weiss” mean field⁹ \mathcal{G}_σ^{-1} in the form of a Dyson equation

$$[G_\sigma(i\omega_n)]^{-1} = [\mathcal{G}_\sigma(i\omega_n)]^{-1} - \Sigma_\sigma(i\omega_n) \quad (1.35)$$

$$= i\omega_n + \mu - \Delta_\sigma(i\omega_n) - \Sigma_\sigma(i\omega_n). \quad (1.36)$$

Then the lattice Green function (in \mathbf{k} -space) $G_{\mathbf{k}\sigma}(i\omega_n)$ is given by

$$G_{\mathbf{k}\sigma}(i\omega_n) = \frac{1}{i\omega_n - \epsilon_{\mathbf{k}} + \mu - \Sigma_\sigma(i\omega_n)}. \quad (1.37)$$

After performing the so-called lattice Hilbert transform we recover the local Green function

⁹ In principle, any one of the local functions $\mathcal{G}_\sigma(i\omega_n)$, $\Sigma_\sigma(i\omega_n)$, or $\Delta_\sigma(i\omega_n)$ can be viewed as a “dynamical mean field” acting on particles on a site, since they all appear in the bilinear term of the local action (1.32).

$$G_\sigma(i\omega_n) = \sum_{\mathbf{k}} G_{\mathbf{k}\sigma}(i\omega_n) = \sum_{\mathbf{k}} \frac{1}{i\omega_n - \epsilon_{\mathbf{k}} + \mu - \Sigma_\sigma(i\omega_n)} \quad (1.38)$$

$$= \int_{-\infty}^{\infty} d\epsilon \frac{N(\omega)}{i\omega_n - \epsilon + \mu - \Sigma_\sigma(i\omega_n)}. \quad (1.39)$$

The ionic lattice on which the electrons move, and its structure, are seen to enter only via the DOS of the non-interacting electrons. After analytic continuation to real frequencies the local (“ \mathbf{k} averaged”) propagator reads

$$G_{\mathbf{k}\sigma}(\omega) = \frac{1}{\omega - \epsilon_{\mathbf{k}} + \mu - \Sigma_\sigma(\omega)}. \quad (1.40)$$

This completes the derivation of the self-consistent DMFT equations. Namely, the functional integral determining the local propagator

$$G_\sigma(i\omega_n) = -\frac{1}{\mathcal{Z}} \int \prod_{\sigma} Dc_{\sigma}^* Dc_{\sigma} [c_{\sigma}(i\omega_n) c_{\sigma}^*(i\omega_n)] \exp[-S_{\text{loc}}], \quad (1.41)$$

where the partition function \mathcal{Z} and the local action S_{loc} are given by

$$\mathcal{Z} = \int \prod_{\sigma} Dc_{\sigma}^* Dc_{\sigma} \exp[-S_{\text{loc}}] \quad (1.42)$$

and (1.32), respectively, together with the expression (1.39) for the lattice Green function provide a closed set of equations for the local propagator $G_\sigma(i\omega_n)$ and the self-energy $\Sigma_\sigma(i\omega_n)$. These equations can be solved iteratively: Starting with an initial value for the self-energy one obtains the local propagator from (1.39) and thereby the bath Green function $\mathcal{G}_\sigma(i\omega_n)$ from (1.35). This determines the local action (1.32) which is used to solve the single-impurity problem (1.41), leading to a new value for the local propagator and, by employing the old self-energy, a new bath Green function, etc. The single-impurity problem is still a complicated many-body interacting problem which cannot, in general, be solved exactly.

1.3.2 Solution of the Self-Consistency Equations of the DMFT

Due to the purely on-site interaction in the local action (1.32) the dynamics of the Hubbard model, (1.1), remains complicated even in the limit $d \rightarrow \infty$. Exact evaluations are only feasible when there is no coupling between the frequencies as, for example, in the Falicov-Kimball model [36]. This model was solved analytically by Brandt and Mielsch [19] soon after the introduction of the $d \rightarrow \infty$ limit [12].

In general, the local action (1.32) is the most complicated part of the DMFT equations. To solve the self-consistency equations different techniques (“impurity solvers”) have been developed which are either fully numerical and “numerically exact”, or semi-analytic and approximate. The numerical solvers can be divided into renormalization group techniques such as the numerical renormalization group (NRG) [37, 38] and the density-matrix renormalization group (DMRG) [39], exact diagonalization (ED) [40–42], and methods based on the stochastic sampling of quantum and thermal averages, i.e., quantum Monte-Carlo (QMC) techniques such as the Hirsch-Fye QMC algorithm [32, 43, 44, 33] and continuous-time (CT) QMC [45–47].

Semi-analytic approximations such as the iterated perturbation theory (IPT) [31, 48, 33], the non-crossing approximation (NCA) [33, 49], the fluctuation exchange approximation (FLEX) [50–53], the local moment approach (LMA) [54, 55], and the parquet approximation [56] can also provide valuable insight.

It quickly turned out that the DMFT is a powerful tool for the investigation of electronic systems with strong correlations. It provides a non-perturbative and thermodynamically consistent approximation scheme for finite-dimensional systems which is particularly valuable for the study of intermediate-coupling problems where perturbative techniques fail [57, 33, 58, 59, 8].

1.4 The Mott-Hubbard Metal-Insulator Transition

The correlation induced transition between a paramagnetic metal and a paramagnetic insulator, referred to as “Mott-Hubbard metal-insulator transition (MIT)”, is one of the most intriguing phenomena in condensed matter physics [60–62]. This transition is a consequence of the competition between the kinetic energy of the electrons and their local interaction U . Namely, the kinetic energy prefers the electrons to move (a wave effect) which leads to doubly occupied sites and thereby to interactions between the electrons (a particle effect). For large values of U the doubly occupied sites become energetically very costly. The system may reduce its total energy by localizing the electrons. Hence the Mott transition is a localization-delocalization transition, demonstrating the particle-wave duality of electrons [59].

Mott-Hubbard MITs are found, for example, in transition metal oxides with partially filled bands. For such systems band theory typically predicts metallic behavior. The most famous example is V_2O_3 doped with Cr [63–65]. In particular, below $T = 380$ K the metal-insulator transition in paramagnetic $(V_{0.96}Cr_{0.04})_2O_3$ is of first order [64], with discontinuities in the lattice parameters and in the conductivity. However, the two phases remain isostructural.

Making use of the half-filled, single-band Hubbard model (1.1) the Mott-Hubbard MIT was studied intensively in the past [5, 65, 60–62]. Important early results were obtained by Hubbard [66] within a Green function decoupling scheme, and by Brinkman and Rice [67] within the Gutzwiller variational method [4], both at $T = 0$. Hubbard’s approach yields a continuous splitting of the band into a lower and upper Hubbard band, but cannot describe quasiparticle features. By contrast, the Gutzwiller-Brinkman-Rice approach gives a good description of the low-energy, quasiparticle behavior, but cannot reproduce the upper and lower Hubbard bands. In the latter approach the MIT is signalled by the disappearance of the quasiparticle peak.

To solve this problem the DMFT has been extremely valuable since it provided detailed insights into the nature of the Mott-Hubbard MIT for all values of the interaction U and temperature T [33, 59].

1.4.1 DMFT and the Three-Peak Structure of the Spectral Function

The Mott-Hubbard MIT is monitored by the spectral function $A(\omega) = -\frac{1}{\pi} \text{Im}G(\omega + i0^+)$ of the correlated electrons¹⁰ [33]. While at small U the

¹⁰ In the following we only consider the paramagnetic phase, whereas magnetic order is assumed to be suppressed (“frustrated”).

system can be described by coherent quasiparticles whose DOS still resembles that of the free electrons, the spectrum in the Mott insulator state consists of two separate incoherent “Hubbard bands” whose centers are separated approximately by the energy U . The latter originate from atomic-like excitations at the energies $\pm U/2$ broadened by the hopping of electrons away from the atom. At intermediate values of U the spectrum then has a characteristic three-peak structure as in the single-impurity Anderson model, which includes both the atomic features (i.e., Hubbard bands) and the narrow quasiparticle peak at low excitation energies, near $\omega = 0$. This corresponds to a strongly correlated metal. The general structure of the spectrum (lower Hubbard band, quasiparticle peak, upper Hubbard band) is rather insensitive to the specific form of the DOS of the non-interacting electrons. The width of the quasiparticle peak vanishes for $U \rightarrow U_{c2}(T)$. On decreasing U , the transition from the insulator to the metal occurs at a lower critical value $U_{c1}(T)$, where the gap vanishes.

It is important to note that the three-peak spectrum originates from a lattice model with only *one* type of electrons. This is in contrast to the single-impurity Anderson model whose spectrum shows very similar features, but is due to *two* types of electrons — the localized orbital at the impurity site and the free conduction band. Therefore the screening of the magnetic moment which gives rise to the Kondo effect in impurity systems has a somewhat different origin in interacting lattice systems. Namely, as explained by the DMFT the electrons provide both the local moments and the electrons which screen these moments [33].

Interestingly, for any typical spectral function $A(\omega)$ with three peaks, Kramers-Kronig relations and the DMFT self-consistency equations imply that the self-energy $\Sigma(\omega)$ abruptly changes slope *inside* the central peak at some frequency ω_* [68], once at positive and once at negative frequency. While this behavior is not visible in $A(\omega)$ itself, it leads to “kinks” in the effective dispersion relation $E_{\mathbf{k}}$ of one-particle excitations, which is defined as the frequency for which the momentum-resolved spectral function $A(\mathbf{k}, \omega) = -\text{Im}G(\mathbf{k}, \omega)/\pi = -(1/\pi) \text{Im}[1/(\omega + \mu - \epsilon_{\mathbf{k}} - \Sigma(\omega))]$ is maximal. For frequencies below ω_* the dispersion is given by Fermi-liquid (FL) theory, $E_{\mathbf{k}} = Z_{\text{FL}}\epsilon_{\mathbf{k}}$, where $Z_{\text{FL}} = (\partial \text{Re}\Sigma(\omega)/\partial \omega)_{\omega=0}$ is the FL renormalization parameter. The FL regime terminates at the kink energy scale ω_* . This energy cannot be obtained within FL theory itself. Namely, it is determined by Z_{FL} and the non-interacting DOS, e.g., $\omega_* = 0.41 Z_{\text{FL}} D$, where D is an energy scale of the non-interacting system such as half the bandwidth [68]. Above ω_* the dispersion is given by a different renormalization with a small offset, $E_{\mathbf{k}} = Z_{\text{CP}}\epsilon_{\mathbf{k}} + \text{const}$, where Z_{CP} is the weight of the central peak of $A(\omega)$. This theory explains kinks in the slope of the dispersion as a direct consequence of the electronic interaction [68]. The same mechanism may also lead to kinks in the low-temperature electronic specific heat [69]. These kinks have also been linked to maxima in the spin susceptibility [70]. Of course, *additional* kinks in the electronic dispersion may also arise from the coupling of electrons to bosonic degrees of freedom, such as phonons [71, 72] or spin fluctuations [73, 74]. Interestingly, recent experiments [75] have found evidence for kinks in Ni(110), which may be due to the electronic mechanism discussed here.

The evolution of the spectral function of the half-filled frustrated Hubbard model at a finite temperature is shown in Fig. 1.2. This temperature is above the temperature of the critical point so that there is no real transition but only a crossover from a metallic-like to an insulating-like solution. The height of the

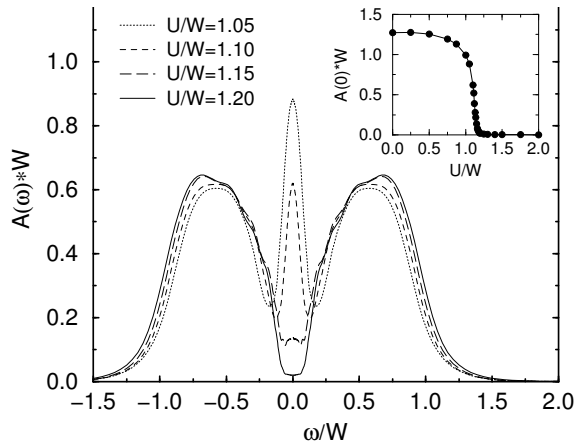


Fig. 1.2. Spectral function for the half-filled Hubbard model for various values of U at $T = 0.0276 W$ (W : bandwidth) in the crossover region. The crossover from the metal to the insulator occurs via a gradual suppression of the quasiparticle peak at $\omega = 0$. The inset shows the U dependence of $A(\omega = 0)$, in particular the rapid decrease for $U \approx 1.1 W$; from Ref. [76].

quasiparticle peak at the Fermi energy is no longer fixed at its zero temperature value. This is due to the temperature dependent imaginary part of the self-energy. The spectral weight of the quasiparticle peak is seen to be gradually redistributed and shifted to the upper (lower) edge of the lower (upper) Hubbard band. The inset of Fig. 1.2 shows the U -dependence of the spectral function at zero frequency $A(\omega = 0)$. For higher values of U the spectral density at the Fermi level is still finite and vanishes only in the limit $U \rightarrow \infty$. For the insulating phase DMFT predicts the filling of the Mott-Hubbard gap with increasing temperature. This is due to the fact that the insulator and the metal are not distinct phases in the crossover regime, implying that the insulator has a finite spectral weight at the Fermi level. This behavior has been detected experimentally by photoemission experiments [77].

Altogether, the thermodynamic transition line $U_c(T)$ corresponding to the Mott-Hubbard MIT is found to be of first order at finite temperatures, and is associated with a hysteresis region in the interaction range $U_{c1} < U < U_{c2}$, where U_{c1} and U_{c2} are the interaction values at which the insulating and metallic solution, respectively, vanish [33, 37, 78, 79, 76, 80]. As shown in Fig. 1.3 the hysteresis region terminates at a critical end point. At higher temperatures the transition changes into a smooth crossover from a bad metal to a bad insulator. At half filling and for bipartite lattices in dimensions $d > 2$ (in $d = 2$ only at $T = 0$) the paramagnetic phase is, in fact, unstable against antiferromagnetic long-range order. The metal-insulator transition is then completely hidden by the antiferromagnetic insulating phase [81].

In Fig. 1.3 it is seen that the slope of the phase transition line U_c is negative down to $T = 0$, which implies that for constant interaction U the metallic phase can be reached from the insulator by decreasing the temperature T , i.e., by cooling. This anomalous behavior (which corresponds to the Pomeranchuk effect [82] in ^3He , if we associate solid ^3He with the insulator and liquid ^3He with the metal) can be understood from the Clausius-Clapeyron equation $dU/dT = \Delta S/\Delta D$. Here ΔS is the difference between the entropy in the metal

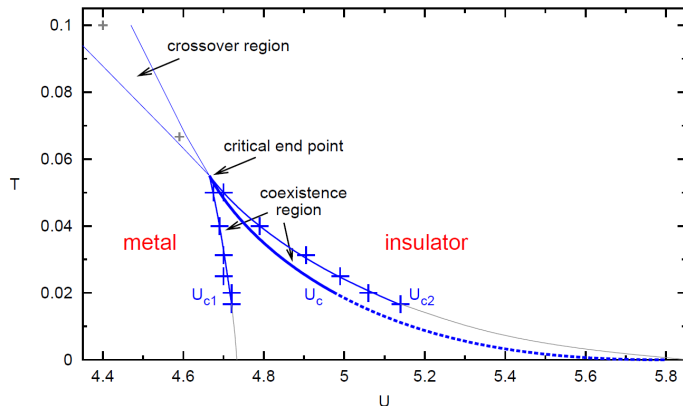


Fig. 1.3. Phase diagram of the Mott-Hubbard MIT showing the metallic phase and the insulating phase, respectively, at temperatures below the critical end point, as well as a coexistence region; from Ref. [80].

and in the insulator, and ΔD is the difference between the number of doubly occupied sites in the two phases. Within the DMFT there is no exchange coupling J between the spins of the electrons in the insulator, since the scaling (1.5) implies $J \propto -t^2/U \propto 1/d \rightarrow 0$ for $d \rightarrow \infty$. Hence the insulating state is macroscopically degenerate, with entropy $S_{\text{ins}} = k_B \ln 2$ per electron down to $T = 0$. This is larger than the entropy $S_{\text{met}} \propto T$ per electron in the Landau Fermi liquid describing the metal, i.e., $\Delta S = S_{\text{met}} - S_{\text{ins}} < 0$. At the same time the number of doubly occupied sites is lower in the insulator than in the metal, i.e., $\Delta D = D_{\text{met}} - D_{\text{ins}} > 0$. The Clausius-Clapeyron equation then implies that the phase-transition line T vs. U has indeed a negative slope down to $T = 0$. However, this is an artifact of the DMFT. Namely, there will usually exist an exchange coupling between the electrons which leads to a vanishing entropy of the insulator for $T \rightarrow 0$. Since the entropy of the insulator vanishes faster than linearly with the temperature, the difference $\Delta S = S_{\text{met}} - S_{\text{ins}}$ eventually becomes positive, whereby the slope also becomes positive¹¹; this is indeed observed in cluster DMFT calculations [83]. However, since $\Delta S \rightarrow 0$ for $T \rightarrow 0$ the phase boundary must eventually terminate at $T = 0$ with infinite slope.

1.5 Theory of Electronic Correlations in Materials

1.5.1 The LDA+DMFT Approach

Although the Hubbard model is able to explain basic features of the phase diagram of correlated electrons it cannot describe the physics of real materials in any detail. Clearly, realistic theories must take into account the explicit electronic and lattice structure of the systems.

Until recently the electronic properties of solids were investigated by two essentially separate communities, one using model Hamiltonians in conjunction with many-body techniques, the other employing density functional theory (DFT) [84, 85]. DFT and its local density approximation (LDA) have

¹¹ Here we assume for simplicity that the metal remains a Fermi liquid and the insulator stays paramagnetic down to the lowest temperatures.

the advantage of being *ab initio* approaches which do not require empirical parameters as input. Indeed, they are highly successful techniques for the calculation of the electronic structure of real materials [86]. However, in practice DFT/LDA is seriously restricted in its ability to describe strongly correlated materials where the on-site Coulomb interaction is comparable with the band width. Here, the model Hamiltonian approach is more powerful since there exist systematic theoretical techniques to investigate the many-electron problem with increasing accuracy. Nevertheless, the uncertainty in the choice of the model parameters and the technical complexity of the correlation problem itself prevent the model Hamiltonian approach from being a suitable tool for studying real materials. The two approaches are therefore complementary. In view of the individual power of DFT/LDA and the model Hamiltonian approach, respectively, a combination of these techniques for *ab initio* investigations of correlated materials including, for example, *f*-electron systems and Mott insulators, would be highly desirable. One of the first successful attempts in this direction was the LDA+U method [87, 88], which combines LDA with a static, i.e., Hartree-Fock-like, mean-field approximation for a multi-band Anderson lattice model with interacting and non-interacting orbitals. This method proved to be a very useful tool in the study of long-range ordered, insulating states of transition metals and rare-earth compounds. However, the paramagnetic metallic phase of correlated electron systems such as high-temperature superconductors and heavy-fermion systems clearly requires a treatment that goes beyond a static mean-field approximation and includes dynamical effects, i.e., the frequency dependence of the self-energy.

Here the recently developed LDA+DMFT method, a new computational scheme which merges electronic band structure calculations and the DMFT, has proved to be a breakthrough [89–94, 49, 59, 52, 95–98]. Starting from conventional band structure calculations in the LDA the correlations are taken into account by the Hubbard interaction and a Hund’s rule coupling term. The resulting DMFT equations are solved numerically, e.g., with a quantum Monte-Carlo (QMC) algorithm. By construction, LDA+DMFT includes the correct quasiparticle physics and the corresponding energetics. It also reproduces the LDA results in the limit of weak Coulomb interaction U . More importantly, LDA+DMFT correctly describes the correlation induced dynamics near a Mott-Hubbard MIT and beyond. Thus, LDA+DMFT is able to account for the physics at all values of the Coulomb interaction and doping level.

In the LDA+DMFT approach the LDA band structure is expressed by a one-particle Hamiltonian \hat{H}_{LDA}^0 , and is then supplemented by the local Coulomb repulsion U and Hund’s rule exchange J . This leads to a material specific generalization of the one-band model Hamiltonian

$$\hat{H} = \hat{H}_{\text{LDA}}^0 + U \sum_m \sum_i \hat{n}_{im\uparrow} \hat{n}_{im\downarrow} + \sum_{i,m \neq m', \sigma, \sigma'} (V - \delta_{\sigma\sigma'} J) \hat{n}_{im\sigma} \hat{n}_{im'\sigma'}. \quad (1.43)$$

Here m and m' enumerate those orbitals for which the interaction between the electrons is explicitly included, e.g., the three t_{2g} orbitals of the $3d$ electrons of transition metal ions or the $4f$ orbitals in the case of rare earth elements. The interaction parameters are related by $V = U - 2J$ which holds exactly for degenerate orbitals and is a good approximation for t_{2g} electrons. The actual values for U and V can be calculated by constrained LDA [49].

In the one-particle part of the Hamiltonian

$$\hat{H}_{\text{LDA}}^0 = \hat{H}_{\text{LDA}} - \sum_i \sum_{m\sigma} \Delta\epsilon_d \hat{n}_{im\sigma}. \quad (1.44)$$

the energy term containing $\Delta\epsilon_d$ is a shift of the one-particle potential of the interacting orbitals. It cancels the Coulomb contribution to the LDA results, and can also be calculated by constrained LDA [49].

Within the LDA+DMFT scheme the self-consistency condition connecting the self-energy Σ and the Green function G at frequency ω reads:

$$G_{qm,q'm'}(\omega) = \frac{1}{V_B} \int d^3k \left([\omega \mathbf{1} + \mu \mathbf{1} - H_{\text{LDA}}^0(\mathbf{k}) - \Sigma(\omega)]^{-1} \right)_{qm,q'm'} \quad (1.45)$$

Here, $\mathbf{1}$ is the unit matrix, μ the chemical potential, $H_{\text{LDA}}^0(\mathbf{k})$ is the orbital matrix of the LDA Hamiltonian derived, for example, in a linearized muffin-tin orbital (LMTO) basis, $\Sigma(\omega)$ denotes the self-energy matrix which is nonzero only between the interacting orbitals, and $[\dots]^{-1}$ implies the inversion of the matrix with elements n ($=qm$), n' ($=q'm'$), where q and m are the indices of the atom in the primitive cell and of the orbital, respectively¹². The integration extends over the Brillouin zone with volume V_B .

For cubic transition metal oxides Eq. (1.45) can be simplified to

$$G(\omega) = G^0(\omega - \Sigma(\omega)) = \int d\epsilon \frac{N^0(\epsilon)}{\omega - \Sigma(\omega) - \epsilon} \quad (1.46)$$

provided the degenerate t_{2g} orbitals crossing the Fermi level are well separated from the other orbitals [49]. For non-cubic systems the degeneracy is lifted. In this case eq. (1.46) is an approximation where different $\Sigma_m(\omega)$, $N_m^0(\epsilon)$ and $G_m(\omega)$ have to be used for the three non-degenerate t_{2g} orbitals.

The Hamiltonian (1.43) is diagonalized within the DMFT where, for example, quantum Monte-Carlo (QMC) techniques [35] are used to solve the self-consistency equations. From the imaginary time QMC Green function we calculate the physical (real frequency) spectral function with the maximum entropy method [99].

During the last few years the LDA+DMFT and other DMFT based computational schemes have provided great progress in the understanding of the electronic, magnetic and structural properties of many correlated electron materials. These materials range from 3d transition metals and their oxides, and f electron systems, all the way to Heusler alloys, ferromagnetic half-metals, fullerenes, and zeolites [52, 95–98]. Nevertheless, this framework still needs to be considerably improved before it becomes a truly comprehensive *ab initio* approach for complex correlated matter with predictive power. In particular, the interface between the band-structure and the many-body components of the approach needs to be optimized. This includes, for example, a solution of the double counting correction problem and a fully self-consistent treatment of the spin, orbital, and charge densities. Another important goal are realistic computations of free energies and forces, and the development of efficient methods to treat non-local correlations with quantum cluster methods [100–102].

1.5.2 Single-Particle Spectrum of Correlated Electrons in Materials

Transition metal oxides are an ideal laboratory for the study of electronic correlations in solids. Among these materials, cubic perovskites have the simplest

¹² We note that \hat{H}_{LDA}^0 may include additional non-interacting orbitals.

crystal structure and thus may be viewed as a starting point for understanding the electronic properties of more complex systems. Typically, the $3d$ states in those materials form comparatively narrow bands with width $W \sim 2-3$ eV, which leads to strong Coulomb correlations between the electrons. Particularly simple are transition metal oxides with a $3d^1$ configuration since, among others, they do not show a complicated multiplet structure.

Photoemission spectra provide a direct experimental tool to study the electronic structure and spectral properties of electronically correlated materials. Intensive experimental investigations of spectral and transport properties of strongly correlated $3d^1$ transition metal oxides started with investigations by Fujimori *et al.* [103]. These authors observed a pronounced lower Hubbard band in the photoemission spectra which cannot be explained by conventional band structure theory. In photoemission spectroscopy (PES) a photon of a given energy is used to emit an electron whose properties (energy, angular distribution) are measured by a detector. Angular resolved PES is referred to as ARPES. These techniques measure the *occupied* electronic states, i.e., those states which are described by the full spectral function multiplied by the Fermi function $f(\omega, T)$. By contrast, inverse photoemission spectroscopy (IPES) measures the *unoccupied* electronic states, i.e., the states described by the full spectral function of a material multiplied by $1 - f(\omega, T)$. IPES is harder to perform and not as accurate as PES. But in many situations information about the unoccupied states is also available by X-ray absorption spectroscopy (XAS).

Spectroscopic techniques provide very valuable information about correlated electronic systems since they can directly measure the spectral function of a material, a quantity which can also be directly calculated as discussed in sec. 1.4. In particular, photoemission techniques allow one to detect the correlation induced shift of spectral weight. In the following we will illustrate the computation of the \mathbf{k} -integrated electronic spectra of correlated materials within the LDA+DMFT scheme by investigating the two simple transition metal oxides SrVO_3 and CaVO_3 .

$\text{Sr}_x\text{Ca}_{1-x}\text{VO}_3$

SrVO_3 and CaVO_3 are simple transition metal compounds with a $3d^1$ configuration. The main effect of the substitution of Sr ions by the isovalent, but smaller, Ca ions is to decrease the V-O-V angle from $\theta = 180^\circ$ in SrVO_3 to $\theta \approx 162^\circ$ in the orthorhombically distorted structure of CaVO_3 . Remarkably this rather strong bond bending results only in a 4% decrease of the one-particle bandwidth W and thus in a correspondingly small increase of the ratio U/W as one moves from SrVO_3 to CaVO_3 [104, 105].

LDA+DMFT(QMC) spectral functions of SrVO_3 and CaVO_3 were calculated by Sekiyama *et al.* [104] by starting from the respective LDA DOS of the two materials; they are shown in Fig. 1.4. These spectra show genuine correlation effects, i.e., the formation of lower Hubbard bands at about 1.5 eV and upper Hubbard bands at about 2.5 eV, with well-pronounced quasiparticle peaks at the Fermi energy. Therefore both SrVO_3 and CaVO_3 are strongly correlated metals. The small difference of the LDA bandwidth of SrVO_3 and CaVO_3 is only reflected in some additional transfer of spectral weight from the quasiparticle peak to the Hubbard bands, and minor differences in the positions of the Hubbard bands. The DOS of the two systems shown in Fig. 1.4 are quite similar. In fact, SrVO_3 is slightly less correlated than CaVO_3 , in

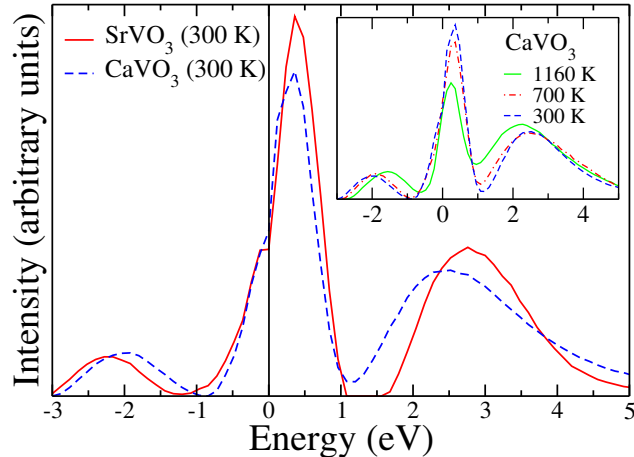


Fig. 1.4. LDA+DMFT(QMC) spectral functions of SrVO_3 (solid line) and CaVO_3 (dashed line) calculated at $T=300$ K; inset: effect of temperature in the case of CaVO_3 ; after Ref. [104].

accord with their different LDA bandwidths. The inset of Fig. 1.4 shows that the effect of temperature on the spectrum is weak for $T \lesssim 700$ K. Detailed spectra of SrVO_3 and CaVO_3 were also computed by Pavarini *et al.* [106].

Since the three t_{2g} orbitals of this simple $3d^1$ material are almost degenerate the spectral function has the same three-peak structure as that of the one-band Hubbard model shown in Fig. 1.2. The temperature induced decrease of the quasiparticle peak height is also clearly seen. We note that the actual form of the spectrum no longer resembles the LDA DOS used as input, i.e., it essentially depends only on the first three energy moments of the LDA DOS (electron density, average energy, band width).

In the left panel of Fig. 1.5 the LDA+DMFT(QMC) spectral functions at 300K are compared with experimental high-resolution bulk PES. For this purpose the full theoretical spectra were multiplied with the Fermi function at the experimental temperature (20 K) and were Gauss broadened with the experimental resolution of 0.1 eV [104]. The quasiparticle peaks in theory and experiment are seen to be in very good agreement. In particular, their height and width are almost identical for both SrVO_3 and CaVO_3 . The difference in the positions of the lower Hubbard bands may be partly due to (i) the subtraction of the estimated oxygen contribution (which may also remove some $3d$ spectral weight below -2 eV), and (ii) uncertainties in the *ab initio* calculation of the local Coulomb interaction strength. In the right panel of Fig. 1.5 comparison is made with XAS data of Inoue *et al.* [107]. To this end the full LDA+DMFT spectrum was multiplied with the inverse Fermi function at 80K and was then Gauss broadened with the experimental resolution of 0.36 eV [108]. The overall agreement of the weights and positions of the quasiparticle and upper t_{2g} Hubbard band is good, including the tendencies when going from SrVO_3 to CaVO_3 (in fact, $\text{Ca}_{0.9}\text{Sr}_{0.1}\text{VO}_3$ in the experiment). For CaVO_3 the weight of the quasiparticle peak is somewhat lower than in the experiment. In contrast to one-band Hubbard model calculations, the material specific results reproduce the strong asymmetry around the Fermi energy w.r.t. weights and bandwidths.

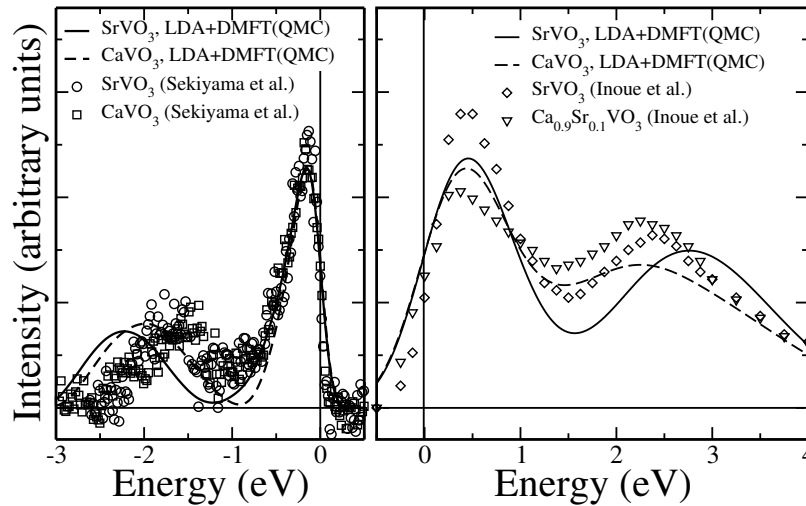


Fig. 1.5. Comparison of the calculated, parameter-free LDA+DMFT(QMC) spectral functions for SrVO₃ (solid line) and CaVO₃ (dashed line) with experiment. Left: Bulk-sensitive high-resolution PES (SrVO₃: circles; CaVO₃: rectangles). Right: 1s XAS for SrVO₃ (diamonds) and Ca_{0.9}Sr_{0.1}VO₃ (triangles) [107]. Horizontal line: experimental subtraction of the background intensity; after Ref. [105].

The experimentally determined spectra of SrVO₃ and CaVO₃ and the good agreement with parameter-free LDA+DMFT calculations confirm the existence of a pronounced three-peak structure in a correlated bulk material. Although the DMFT had predicted such a behavior for the Hubbard model [33] it was not clear whether the DMFT would really be able to describe real materials. Now it is clear that the three-peak structure not only occurs in single-impurity Anderson models or the DMFT for the Hubbard model, but is also a characteristic feature of correlated *bulk* matter in $d = 3$.

1.6 Electronic Correlations and Disorder

The properties of real materials are influenced not only by the interaction between the electrons in the periodic crystal lattice, but also by the presence of randomness, e.g., impurities and lattice defects [109]. In particular, Coulomb correlations and disorder are separately driving forces behind metal-insulator transitions (MITs) connected with the localization and delocalization of particles. The Mott-Hubbard MIT is caused by the electronic repulsion [110,5,61] and is characterized by the opening of a gap in the density of states at the Fermi level. By contrast, the Anderson localization transition is due to coherent backscattering of non-interacting particles from randomly distributed impurities [111,109]. At the Anderson transition the character of the spectrum at the Fermi level changes from a continuous to a dense point spectrum. Both MITs can be characterized by a single quantity, the local density of states (LDOS). Although the LDOS is not an order parameter associated with a symmetry-breaking phase transition, it can distinguish between a metal and an insulator.

The DMFT can easily be extended to study correlated lattice electrons with local disorder [112–117, 8]. For this purpose a single-particle term with random local energies ϵ_i is added to the Hubbard model, leading to the Anderson-Hubbard model

$$\hat{H} = -t \sum_{ij,\sigma} \hat{c}_{i\sigma}^\dagger \hat{c}_{j\sigma} + \sum_{i\sigma} \epsilon_i n_{i\sigma} + U \sum_i \hat{n}_{i\uparrow} \hat{n}_{i\downarrow}. \quad (1.47)$$

The ionic energies ϵ_i describe the local, quenched disorder acting on the motion of the electrons. They are drawn from a probability distribution function $\mathcal{P}(\epsilon_i)$, which can be a continuous or a multi-modal function.

The DMFT provides a valuable, non-perturbative theoretical framework also for the investigation of correlated electrons in the presence of disorder. If in the DMFT the effect of local disorder is taken into account through the arithmetic mean of the LDOS one obtains, in the absence of interactions ($U = 0$), the coherent potential approximation (CPA) [30, 118], which does not describe the physics of Anderson localization. To overcome this deficiency Dobrosavljević and collaborators formulated a variant of the DMFT where the *geometrically* averaged LDOS is computed from the solutions of the self-consistent stochastic DMFT equations [119] which is then incorporated into the self-consistency cycle [120]. Thereby a mean-field theory of Anderson localization can be derived which reproduces many of the expected features of the disorder-driven MIT for non-interacting electrons [120]. This scheme uses only one-particle quantities and can therefore easily be included in the DMFT to treat disordered electrons in the presence of phonons [121] or Coulomb correlations [122, 123]. In particular, the DMFT with geometrical averaging allows one to compute the phase diagram for the Anderson-Hubbard model [122, 123]. For a continuous disorder distribution function and a half filled band one finds that the metallic phase is *enhanced* at small and intermediate values of the interaction and disorder, but that the metallicity is eventually destroyed when the disorder is strong enough [122]. Surprisingly, the Mott and Anderson insulators are continuously connected.

New interesting phenomena are also expected in correlated electron systems when the disorder distribution function has a binary-alloy form. Namely, it was predicted that a disorder induced splitting of the band (“alloy-band splitting”) can enhance the critical temperature for the onset of itinerant ferromagnetism [124, 125]. Another direct consequence of the alloy-band splitting is the fact that, if the alloy subband is effectively half-filled, a Mott-Hubbard metal-insulator transition can occur at non-integer filling [126]. The spectral-weight transfer in correlated systems with binary-alloy disorder was also investigated away from the metal-insulator transition regime [127, 128]. For the periodic Anderson model with the binary-alloy disorder analogous behavior was predicted [129].

1.7 DMFT for Correlated Bosons in Optical Lattices

The observation of Bose-Einstein condensation (BEC) in ultra-cold atomic gases has greatly stimulated research into the properties of this fascinating quantum state of matter [130]. In particular, experiments with alkali atoms confined in optical lattices [131–133] have renewed the theoretical interest [134–136] in the physics of strongly correlated bosons on lattices, which

promises significant new insights and even applications in fields such as quantum computing [137].

A lattice model of interacting bosons with purely local interaction, the bosonic Hubbard model, has the form

$$H_{\text{BH}} = \sum_{\langle i,j \rangle} t_{ij} \hat{b}_i^\dagger \hat{b}_j + \frac{U}{2} \sum_{\mathbf{R}_i} \hat{n}_i (\hat{n}_i - 1), \quad (1.48)$$

where \hat{b}_i and \hat{b}_i^\dagger are bosonic operators. In the ground state two characteristically different phases are expected to occur: a bosonic incompressible Mott phase with a correlation gap and a compressible superfluid phase characterized by a non-vanishing expectation value $\langle \hat{b}_i \rangle$ which serves as an order parameter [138].

The construction of a DMFT for the bosonic Hubbard model which — as in the case of the fermionic DMFT — becomes exact in the limit d or $Z \rightarrow \infty$ and is valid at all temperatures is made complicated by the fact that the system can Bose condense below a Bose-Einstein condensation temperature T_{BEC} . This has immediate consequences for the expectation value of the kinetic energy in (1.48). Namely, while in the normal state only the product $\hat{b}_i^\dagger \hat{b}_j$ has a finite expectation value, in the Bose condensed phase even $\langle \hat{b}_j \rangle$ (the order parameter) is non-zero. For the expectation value of the kinetic energy in (1.48) to remain finite in the limit $Z \rightarrow \infty$ the hopping amplitude then has to be scaled differently in the two phases. In the normal phase the hopping amplitude needs to be scaled as in the fermionic case (“quantum scaling”), i.e., as $t_{ij} = t_{ij}^*/\sqrt{Z}$, while in the condensed phase a classical scaling $t_{ij} = t_{ij}^*/Z$ is required. Such a scaling of the hopping amplitudes cannot be performed on the level of the Hamiltonian, but is possible in the effective action [139]. The bosonic DMFT (“B-DMFT”) derived thereby treats normal and condensed bosons on equal footing and thus includes the effects caused by their dynamic coupling. The self-consistency equations of the B-DMFT are those of a single bosonic impurity coupled to two baths, one corresponding to bosons in the normal state and one to bosons in the condensate. The B-DMFT derived in the limit d or $Z \rightarrow \infty$ is again a comprehensive mean-field theory, i.e., it is valid for all input parameters and all temperatures. It not only reproduces all exactly solvable limits, such as the non-interacting ($U = 0$) and the atomic ($t_{ij} = 0$) limit, but also well-known approximation schemes for interacting bosons. For example, by neglecting all terms containing the hybridization function in the local action one obtains the mean-field theory of Fisher *et al.* [138]; for a detailed discussion see [139].

The solution of the self-consistent bosonic impurity problem defined by the B-DMFT equations requires new theoretical/computational methods. So far exact diagonalization [140, 141] and continuous-time QMC [142] were employed. Thereby the bosonic Hubbard model was solved on the Bethe lattice for finite [140] and infinite [141] coordination number Z as well as on a simple-cubic lattice [142]. The phase diagram of correlated bosons on a simple-cubic lattice computed by the bosonic DMFT was found to agree with that obtained by numerically exact QMC to within 2% [142].

The B-DMFT is expected to be a valuable approximation scheme for the investigation of lattice bosons in situations where exact numerical computations are difficult to perform or inefficient, as in the case of bosons with disorder or many internal degrees of freedom, and for Bose-Fermi mixtures [143].

1.8 DMFT for Nonequilibrium

Recently the study of strongly correlated many-body systems out of equilibrium has received much attention [144, 145]. This is motivated in particular by experimental progress in the investigation of ultra-cold atomic gases [133] and time-resolved pump-probe spectroscopy on strongly correlated materials [146, 147]. In general the real-time dynamics of correlated systems can be described by the extension of DMFT to nonequilibrium, provided that they are dominated by local temporal fluctuations and spatial correlations are not crucial. In nonequilibrium DMFT an effective impurity problem is formulated using the Keldysh formalism [148, 149], and as in equilibrium DMFT this mapping onto a single site becomes exact in the limit of infinite dimensions. For the Hubbard model in nonequilibrium the single-site DMFT action reads

$$S = -i \int_{\mathcal{C}} dt H_{\text{loc}}(t) - i \sum_{\sigma} \int_{\mathcal{C}} dt \int_{\mathcal{C}} dt' c_{\sigma}^{\dagger}(t) \Lambda(t, t') c_{\sigma}(t'), \quad (1.49)$$

where the Keldysh contour \mathcal{C} runs from t_{\min} to t_{\max} on the real time axis, back to t_{\min} , and finally to $-i\beta$ along the imaginary time axis [150, 151]. The first term contains the local part of the Hamiltonian, e.g., $H_{\text{loc}}(t) = U(t)n_{\uparrow}n_{\downarrow} - \mu(n_{\uparrow} + n_{\downarrow})$ for a time-dependent interaction. The second term involves the hybridization function $\Lambda(t, t')$ which couples the impurity to a time-dependent bath which must be determined self-consistently. Local contour-ordered correlation functions such as the Green function $G(t, t')$ are obtained from the action (1.49) as expectation values $\langle A(t)B(t') \dots \rangle = \text{Tr}[\mathbb{T}_{\mathcal{C}} \exp(S)A(t)B(t') \dots] / \mathcal{Z}$ at the appropriate times, where $\mathbb{T}_{\mathcal{C}}$ is the contour-ordering operator. For the Hubbard model this evaluation is the most demanding part of nonequilibrium DMFT and can so far be done with real-time quantum Monte Carlo methods [152, 151] for not too long times, and for sufficiently large U using a self-consistent perturbation expansion around the atomic limit [153]. For the Falicov-Kimball model, on the other hand, closed equations of motion govern the impurity Green function [19], which can be solved on the real time axis. The hybridization function $\Lambda(t, t')$ in eq. (1.49) must be determined self-consistently by computing the local self-energy $\Sigma(t, t')$ from the Dyson equation of the impurity model, calculating the momentum-dependent Green function of the lattice model from the lattice Dyson equation, integrating over momentum to obtain the local lattice Green function, and finally equating it with the impurity Green function. While this procedure is necessary for a Gaussian or other general DOS, for a semielliptical DOS the self-energy can be eliminated and Λ expressed directly in terms of G [154].

Nonequilibrium DMFT was used to obtain the response of time-resolved photoemission [155–157] and optical spectroscopy [158] in correlated systems in terms of Green functions of the electronic system. The Falicov-Kimball and Hubbard models were studied in the presence of dc and ac electric fields [149, 159–166, 157], as well as for abrupt [167, 158, 156, 152, 151, 153] or slow changes [168, 169] of the interaction parameter as a function of time.

As an example, we consider a sudden change (“quench”) in the interaction parameter of the Hubbard model from $U = 0$ (i.e., with the non-interacting ground state as initial state) to finite values of U for times $t > 0$. For this case the DMFT equations were solved numerically for the paramagnetic phase and a semielliptic DOS [152, 151, 153]. In the following discussion the bandwidth

is equal to 4, and time is thus measured in units of $4\hbar/\text{bandwidth}$, e.g., on the order of femto-seconds for a bandwidth on the order of eV. An interesting question is whether such an isolated system can thermalize due to the many-body interaction alone, i.e., whether at least some of its properties are the same as for an equilibrium system with the same energy [170]. Before the quench the momentum distribution is a step function, and the Fermi surface discontinuity $\Delta n(t)$ remains nonzero for a finite time after the quench. For quenches to $U \lesssim 2.5$ the momentum discontinuity first reaches a so-called prethermalization plateau for $t \lesssim 5$ due to the vicinity of the integrable point at $U = 0$. This plateau in $\Delta n(t)$ is given to good accuracy by $2Z - 1$ [152], where Z is the Fermi-liquid quasiparticle weight *in equilibrium* at zero temperature and for interaction U . This value and also the transient behavior at short times is precisely predicted by second-order unitary perturbation theory in U [171, 172]. On the other hand, the double occupation essentially relaxes to its thermal value on this timescale, showing that the potential energy (and therefore also the kinetic energy) relax quicker than the occupation of individual states. For large U the behavior is different, showing strong so-called collapse-and-revival oscillations with approximate frequency $2\pi/U$. They stem from the vicinity of the atomic limit (i.e., zero hopping amplitude), for which the propagator e^{-iHt} is exactly periodic with period $2\pi/U$ [173]. For finite hopping (small compared to U) these oscillations are damped and decay on timescales of order $\hbar/\text{bandwidth}$. The oscillations of the double occupation are not centered at its thermal value, but rather at a different value that can be derived from strong-coupling perturbation theory [152]. The situation is thus similar to that at small coupling in the sense that the relaxation to the thermal state is delayed because the system is stuck in a metastable state close to an integrable point. However, both the weak-coupling prethermalization plateau in $\Delta n(t)$ as well as the strong-coupling oscillations vanish in a narrow region of interaction parameters U near 3.2 [152]. For quenches of U to approximately this value the system thermalizes rapidly: Both the momentum distribution and thus also the double occupation (due to energy conservation after quench) relax to their thermal values. In fact the retarded nonequilibrium Green function relaxes to the corresponding equilibrium function [151], so that all observables that can be obtained from it tend to the thermal value predicted by equilibrium statistical mechanics. In other words, for quenches to interaction values in the vicinity of $U \approx 3.2$ the isolated system indeed thermalizes rapidly due to the many-body interactions. Many interesting questions remain open in this context, e.g., how thermalization depends on the parameters of the system. We refer to the reviews [144, 145] for further discussion.

1.9 Summary and Outlook

Due to the intensive international research over the last two decades the DMFT has quickly developed into a powerful method for the investigation of electronic systems with strong correlations. It provides a comprehensive, non-perturbative and thermodynamically consistent approximation scheme for the investigation of finite-dimensional systems (in particular for dimension $d = 3$), and is particularly useful for the study of problems where perturbative approaches are inapplicable. For this reason the DMFT has now become the standard mean-field theory for fermionic correlation problems, including cold atoms in optical lattices [174–176]. The study of models in nonequilib-

rium using an appropriate generalization of DMFT has become yet another fascinating new research area [149, 151–153, 156–169].

Until a few years ago research into correlated electron systems concentrated on homogeneous bulk systems. DMFT investigations of systems with internal or external inhomogeneities such as thin films and multi-layered nanostructures are still very new [177–182, 175]. They are particularly important in view of the novel types of functionalities of such systems, which may have important applications in electronic devices. Here the DMFT and its non-local extensions [100–102] will certainly become very useful.

In particular, the development of the *ab initio* band-structure calculation technique referred to as LDA+DMFT has proved to be a breakthrough in the investigation of electronically correlated materials. It provided already important insights into the spectral and magnetic properties of correlated electron materials [94, 49, 52, 95–97]. Clearly, this approach has a great potential for further developments. Indeed, it is not hard to foresee that the LDA+DMFT framework will eventually develop into a comprehensive *ab initio* approach which is able to describe, and even predict, the properties of complex correlated materials.

Acknowledgments

We thank Jim Allen, Vladimir Anisimov, Nils Blümer, Ralf Bulla, Liviu Chioncel, Theo Costi, Vlad Dobrosavljević, Peter van Dongen, Martin Eckstein, Volker Eyert, Florian Gebhard, Karsten Held, Walter Hofstetter, Vaclav Janiš, Anna Kauch, Stefan Kehrein, Georg Keller, Gabi Kotliar, Jan Kuneš, Ivan Leonov, Walter Metzner, Michael Moeckel, Igor Nekrasov, Thomas Pruschke, Xinguo Ren, Shigemasa Suga, Götz Uhrig, Martin Ulmke, Ruud Vlamming, Philipp Werner, and Unjong Yu for valuable collaborations. Support by the Deutsche Forschungsgemeinschaft through TRR 80 and FOR 1346 is gratefully acknowledged. KB was also supported by the grant N N202 103138 of the Polish Ministry of Science and Education.

References

1. J.H. de Boer, E.J.W. Verwey, Proc. Phys. Soc. **49**, 59 (1937)
2. N.F. Mott, R. Peierls, Proc. Phys. Soc. A **49**, 72 (1937)
3. M. Imada, A. Fujimori, Y. Tokura, Rev. Mod. Phys. **70**, 1039 (1998)
4. M.C. Gutzwiller, Phys. Rev. Lett. **10**, 59 (1963)
5. J. Hubbard, Proc. Roy. Soc. London **A276**, 238 (1963)
6. J. Kanamori, Prog. Theor. Phys. **30**, 275 (1963)
7. E. Lieb, F.Y. Wu, Phys. Rev. Lett. **20**, 1445 (1968)
8. D. Vollhardt, in *Lectures on the Physics of Strongly Correlated Systems XIV, AIP Conference Proceedings*, vol. 1297, ed. by A. Avella, F. Mancini (American Institute of Physics, Melville, 2010), p. 339
9. D. Vollhardt, in *Correlated Electron Systems*, ed. by V.J. Emery (World Scientific, Singapore, 1993), p. 57
10. R.J. Baxter, *Exactly Solved Models in Statistical Mechanics* (Academic Press, London, 1982)
11. C. Itzykson, J.M. Drouffe, *Statistical Field Theory* (Cambridge University Press, Cambridge, 1989)
12. W. Metzner, D. Vollhardt, Phys. Rev. Lett. **62**, 324 (1989)

13. U. Wolff, Nucl. Phys. B **225**, 391 (1983)
14. E. Müller-Hartmann, Z. Phys. B **74**, 507 (1989)
15. W. Metzner, Z. Phys. B **77**, 253 (1989)
16. E. Müller-Hartmann, Z. Phys. B **76**, 211 (1989)
17. H. Schweitzer, G. Czycholl, Solid State Comm. **69**, 171 (1989)
18. H. Schweitzer, G. Czycholl, Z. Phys. B **83**, 93 (1991)
19. U. Brandt, C. Mielsch, Z. Phys. B **75**, 365 (1989)
20. P.G.J. van Dongen, F. Gebhard, D. Vollhardt, Z. Phys. **76**, 199 (1989)
21. F. Kajzar, J. Friedel, J. Phys. (Paris) **39**, 397 (1978)
22. G. Treglia, F. Ducastelle, D. Spanjaard, Phys. Rev. B **22**, 6472 (1980)
23. G. Bulk, R.J. Jelitto, Phys. Rev. B **41**, 413 (1990)
24. J.M. Luttinger, J.C. Ward, Phys. Rev. **118**, 1417 (1960)
25. V. Janiš, Z. Phys. B **83**, 227 (1991)
26. V. Janiš, D. Vollhardt, Int. J. Mod. Phys. B **6**, 731 (1992)
27. B. Velický, S. Kirkpatrick, H. Ehrenreich, Phys. Rev. **175**, 745 (1968)
28. F. Yonezawa, K. Morigaki, Suppl. Prog. Theor. Phys. **53**, 1 (1973)
29. R.J. Elliot, J.A. Krumhansl, P.L. Leath, Rev. Mod. Phys. **46**, 465 (1974)
30. R. Vlaming, D. Vollhardt, Phys. Rev. B **45**, 4637 (1992)
31. A. Georges, G. Kotliar, Phys. Rev. B **45**, 6479 (1992)
32. M. Jarrell, Phys. Rev. Lett. **69**, 168 (1992)
33. A. Georges, G. Kotliar, W. Krauth, M.J. Rozenberg, Rev. Mod. Phys. **68**, 13 (1996)
34. M. Fabrizio, in *Lectures on the Physics of highly correlated electron systems XI, AIP Conference Proceedings*, vol. 918, ed. by A. Avella, F. Mancini (American Institute of Physics, Melville, 2007), p. 3
35. J.E. Hirsch, R.M. Fye, Phys. Rev. Lett. **56**, 2521 (1986)
36. J.K. Freericks, V. Zlatić, Rev. Mod. Phys. **75**, 1333 (2003)
37. R. Bulla, Phys. Rev. Lett. **83**, 136 (1999)
38. R. Bulla, T.A. Costi, T. Pruschke, Rev. Mod. Phys. **80**, 395 (2008)
39. M. Karski, C. Raas, G.S. Uhrig, Phys. Rev. B **77**, 075116 (2008)
40. M. Caffarel, W. Krauth, Phys. Rev. Lett. **72**, 1545 (1994)
41. Q. Si, M.J. Rozenberg, G. Kotliar, A.E. Ruckenstein, Phys. Rev. Lett. **72**, 2761 (1994)
42. M.J. Rozenberg, G. Moeller, G. Kotliar, Mod. Phys. Lett. B **8**, 535 (1994)
43. M.J. Rozenberg, X.Y. Zhang, G. Kotliar, Phys. Rev. Lett. **69**, 1236 (1992)
44. A. Georges, W. Krauth, Phys. Rev. Lett. **69**, 1240 (1992)
45. A.N. Rubtsov, V.V. Savkin, A.I. Lichtenstein, Phys. Rev. B **72**, 035122 (2005)
46. P. Werner, A. Comanac, L. de' Medici, M. Troyer, A.J. Millis, Phys. Rev. Lett. **97**, 076405 (2006)
47. K. Haule, Phys. Rev. B **75**, 155113 (2007)
48. X.Y. Zhang, M.J. Rozenberg, G. Kotliar, Phys. Rev. Lett. **70**, 1666 (1993)
49. K. Held, I.A. Nekrasov, G. Keller, V. Eyert, N. Blümer, A.K. McMahan, R.T. Scalettar, T. Pruschke, V.I. Anisimov, D. Vollhardt, Psi-k Newsletter **56**, 65 (2003). Reprinted in Phys. Status Solidi B **243**, 2599 (2006)
50. N.E. Bickers, D.J. Scalapino, Ann. Phys. (NY) **193**, 206 (1989)
51. A.I. Lichtenstein, M.I. Katsnelson, J. Phys. Condens. Matter **11**, 1037 (1999)
52. G. Kotliar, S.Y. Savrasov, K. Haule, V.S. Oudovenko, O. Parcollet, C.A. Marianetti, Rev. Mod. Phys. **78**, 865 (2006)
53. V. Drchal, V. Janiš, J. Kudrnovský, V.S. Oudovenko, X. Dai, K. Haule, G. Kotliar, J. Phys.: Condens. Matter **17**, 61 (2005)
54. D.E. Logan, M.T. Glossop, J. Phys. Condens. Matter **12**, 985 (2000)
55. A. Kauch, K. Byczuk, ArXiv:0912.4278 (2009)
56. V. Janiš, P. Augustinský, Phys. Rev. B **75**, 165108 (2007)
57. T. Pruschke, M. Jarrell, J.K. Freericks, Adv. Phys. **44**, 187 (1995)
58. A. Georges, in *Lectures on the Physics of highly correlated electron systems VIII, AIP Conference Proceedings*, vol. 715, ed. by A. Avella, F. Mancini (American Institute of Physics, Melville, 2004), p. 3

59. G. Kotliar, D. Vollhardt, *Physics Today* **57**(No. 3 (March)), 53 (2004)
60. N.F. Mott, *Rev. Mod. Phys.* **40**, 677 (1968)
61. N.F. Mott, *Metal-Insulator Transitions*, 2nd edn. (Taylor and Francis, London, 1990)
62. F. Gebhard, *The Mott Metal-Insulator Transition* (Springer, Berlin, 1997)
63. D.B. McWhan, J.P. Remeika, *Phys. Rev. B* **2**, 3734 (1970)
64. D.B. McWhan, A. Menth, J.P. Remeika, W.F. Brinkman, T.M. Rice, *Phys. Rev. B* **7**, 1920 (1973)
65. T.M. Rice, D.B. McWhan, *IBM J. Res. Develop.* **14**, 251 (1970)
66. J. Hubbard, *Proc. Roy. Soc. London* **A281**, 401 (1964)
67. W.F. Brinkman, T.M. Rice, *Phys. Rev. B* **2**, 4302 (1970)
68. K. Byczuk, M. Kollar, K. Held, Y.F. Yang, I.A. Nekrasov, T. Pruschke, D. Vollhardt, *Nature Physics* **3**, 168 (2007)
69. A. Toschi, M. Capone, C. Castellani, K. Held, *Phys. Rev. Lett.* **102**, 076402 (2009)
70. C. Raas, P. Grete, G.S. Uhrig, *Phys. Rev. Lett.* **102**, 076406 (2009)
71. A. Lanzara, P.V. Bogdanov, X.J. Zhou, S.A. Kellar, D.L. Feng, E.D. Lu, T. Yoshida, H. Eisaki, A. Fujimori, K. Kishio, J.I. Shimoyama, T. Noda, S. Uchida, Z. Hussain, Z.X. Shen, *Nature* **412**, 510 (2001)
72. Z.X. Shen, A. Lanzara, S. Ishihara, N. Nagaosa, *Philos. Mag. B* **82**, 1349 (2002)
73. H. He, Y. Sidis, P. Bourges, G.D. Gu, A. Ivanov, N. Koshizuka, B. Liang, C.T. Lin, L.P. Regnault, E. Schoenherr, B. Keimer, *Phys. Rev. Lett.* **86**, 1610 (2001)
74. J. Hwang, T. Timusk, G.D. Gu, *Nature* **427**, 714 (2004)
75. A. Hofmann, X.Y. Cui, J. Schäfer, S. Meyer, P. Höpfner, C. Blumenstein, M. Paul, L. Patthey, E. Rotenberg, J. Bünemann, F. Gebhard, T. Ohm, W. Weber, R. Claessen, *Phys. Rev. Lett.* **102**, 187204 (2009)
76. R. Bulla, T.A. Costi, D. Vollhardt, *Phys. Rev. B* **64**, 045103 (2001)
77. S.K. Mo, H.D. Kim, J.W. Allen, G.H. Gweon, J.D. Denlinger, J.H. Park, A. Sekiyama, A. Yamasaki, S. Suga, P. Metcalf, K. Held, *Phys. Rev. Lett.* **93**, 076404 (2004)
78. M.J. Rozenberg, R. Chitra, G. Kotliar, *Phys. Rev. Lett.* **83**, 3498 (1999)
79. J. Joo, V. Oudovenko, *Phys. Rev. B* **64**, 193102 (2001)
80. N. Blümer, *Metal-Insulator Transition and Optical Conductivity in High Dimensions* (Shaker Verlag, Aachen, 2003)
81. T. Pruschke, *Prog. Theor. Phys. Suppl.* **160**, 274 (2005)
82. D. Vollhardt, P. Wölfle, *The Superfluid Phases of Helium 3* (Taylor and Francis, London, 1990)
83. H. Park, K. Haule, G. Kotliar, *Phys. Rev. Lett.* **101**, 186403 (2008)
84. P. Hohenberg, W. Kohn, *Phys. Rev.* **136B**, 864 (1964)
85. W. Kohn, L.J. Sham, *Phys. Rev.* **140**, A1133 (1965)
86. R.O. Jones, O. Gunnarsson, *Rev. Mod. Phys.* **61**, 689 (1989)
87. V.I. Anisimov, J. Zaanen, O.K. Andersen, *Phys. Rev. B* **44**, 943 (1991)
88. V.I. Anisimov, F. Aryasetiawan, A.I. Lichtenstein, *J. Phys.: Cond. Matter* **9**, 767 (1997)
89. V.I. Anisimov, A.I. Poteryaev, M.A. Korotin, A.O. Anokhin, G. Kotliar, *J. Phys.: Cond. Matter* **9**, 7359 (1997)
90. A.I. Lichtenstein, M.I. Katsnelson, *Phys. Rev. B* **57**, 6884 (1998)
91. I.A. Nekrasov, K. Held, N. Blümer, A.I. Poteryaev, V.I. Anisimov, D. Vollhardt, *Eur. Phys. J. B* **18**, 55 (2000)
92. K. Held, I.A. Nekrasov, N. Blümer, V.I. Anisimov, D. Vollhardt, *Int. J. Mod. Phys. B* **15**, 2611 (2001)
93. K. Held, I.A. Nekrasov, G. Keller, V. Eyert, N. Blümer, A.K. McMahan, R. Scalettar, T. Pruschke, V. Anisimov, D. Vollhardt, in *Quantum Simulations of Complex Many-Body Systems: From Theory to Algorithms*, NIC Series Volume, vol. 10, ed. by J. Grotendorst, D. Marks, A. Muramatsu (NIC Directors, Forschungszentrum Jülich, Berlin, 2002), p. 175

94. A.I. Lichtenstein, M.I. Katsnelson, G. Kotliar, in *Electron Correlations and Materials Properties*, ed. by A. Gonis, N. Kioussis, M. Ciftan (Kluwer Academic/Plenum, New York, 2002), p. 428
95. K. Held, *Adv. Phys.* **56**, 829 (2007)
96. M.I. Katsnelson, V.Y. Irkhin, L. Chioncel, A.I. Lichtenstein, R.A. de Groot, *Rev. Mod. Phys.* **80**, 315 (2008)
97. V. Anisimov and Y. Izyumov, *Electronic Structure of Correlated Materials*, Springer Series in Solid-State Sciences **163** (Springer, Berlin, 2010)
98. J. Kuneš, I. Leonov, M. Kollar, K. Byczuk, V.I. Anisimov, D. Vollhardt, *Eur. Phys. J. Special Topics* **180**, 5 (2010)
99. M. Jarrell, J.E. Gubernatis, *Phys. Rep.* **269**, 133 (1996)
100. M. Potthoff, *Adv. Solid State Phys.* **45**, 135 (2005)
101. T. Maier, M. Jarrell, T. Pruschke, M.H. Hettler, *Rev. Mod. Phys.* **77**, 1027 (2005)
102. K. Held, A.A. Katanin, A. Toschi, *Prog. Theor. Phys. Suppl.* **176**, 117 (2008)
103. A. Fujimori, I. Hase, H. Namatame, Y. Fujishima, Y. Tokura, H. Eisaki, S. Uchida, K. Takegahara, F.M.F. de Groot, *Phys. Rev. Lett.* **69**, 1796 (1992)
104. A. Sekiyama, H. Fujiwara, S. Imada, S. Suga, H. Eisaki, S.I. Uchida, K. Takegahara, H. Harima, Y. Saitoh, I.A. Nekrasov, G. Keller, D.E. Kondakov, A.V. Kozhevnikov, T. Pruschke, K. Held, D. Vollhardt, V.I. Anisimov, *Phys. Rev. Lett.* **93**, 156402 (2004)
105. I.A. Nekrasov, G. Keller, D.E. Kondakov, A.V. Kozhevnikov, T. Pruschke, K. Held, D. Vollhardt, V.I. Anisimov, *Phys. Rev. B* **72**, 155106 (2005)
106. E. Pavarini, S. Biermann, A. Poteryaev, A.I. Lichtenstein, A. Georges, O.K. Andersen, *Phys. Rev. Lett.* **92**, 176403 (2004)
107. I.H. Inoue, I. Hase, Y. Aiura, A. Fujimori, K. Morikawa, T. Mizokawa, Y. Haruyama, T. Maruyama, Y. Nishihara, *Physica C* **235-240**, 1007 (1994)
108. I.H. Inoue, private communication (2003)
109. P.A. Lee, T.V. Ramakrishnan, *Rev. Mod. Phys.* **57**, 287 (1985)
110. N.F. Mott, *Proc. Phys. Soc. London, Sect. A* **62**, 415 (1949)
111. P.W. Anderson, *Phys. Rev.* **109**, 1492 (1958)
112. V. Janiš, D. Vollhardt, *Phys. Rev. B* **46**, 15712 (1992)
113. V. Janiš, M. Ulmke, D. Vollhardt, *Europhysics Letters* **24**, 287 (1993)
114. M. Ulmke, V. Janiš, D. Vollhardt, *Phys. Rev. B* **51**, 10411 (1995)
115. V. Dobrosavljević, G. Kotliar, *Phys. Rev. B* **50**, 1430 (1994)
116. M.C.O. Aguiar, V. Dobrosavljević, E. Abrahams, G. Kotliar, *Phys. Rev. B* **73**, 115117 (2006)
117. M. Potthoff, M. Balzer, *Phys. Rev. B* **75**, 125112 (2007)
118. V. Janiš, D. Vollhardt, *Phys. Rev. B* **46**, 15712 (1992)
119. V. Dobrosavljević, G. Kotliar, *Phys. Rev. Lett.* **78**, 3943 (1997)
120. V. Dobrosavljević, A.A. Pastor, B.K. Nikolić, *Europhys. Lett.* **62**, 76 (2003)
121. F.X. Bronold, A. Alvermann, H. Fehske, *Phil. Mag.* **84**, 637 (2004)
122. K. Byczuk, W. Hofstetter, D. Vollhardt, *Phys. Rev. Lett.* **94**, 056404 (2005)
123. K. Byczuk, W. Hofstetter, D. Vollhardt, *Phys. Rev. Lett.* **102**, 146403 (2009)
124. K. Byczuk, M. Ulmke, D. Vollhardt, *Phys. Rev. Lett.* **90**, 196403 (2003)
125. K. Byczuk, M. Ulmke, *Eur. Phys. J. B* **45**, 449 (2005)
126. K. Byczuk, W. Hofstetter, D. Vollhardt, *Phys. Rev. B* **69**, 045112 (2004)
127. P. Lombardo, R. Hayn, G.I. Japaridze, *Phys. Rev. B* **74**, 085116 (2006)
128. M. Potthoff, M. Balzer, *Phys. Rev. B* **75**, 125112 (2007)
129. U. Yu, K. Byczuk, D. Vollhardt, *Phys. Rev. Lett.* **100**, 246401 (2008)
130. R.J. Anglin, W. Ketterle, *Nature* **416**, 211 (2002)
131. M. Greiner, O. Mandel, T. Esslinger, T.W. Hänsch, I. Bloch, *Nature* **415**, 39 (2002)
132. M. Lewenstein, A. Sanpera, V. Ahufinger, B. Damski, A. Sen, U. Sen, *Advances in Physics* **56**, 243 (2007)
133. I. Bloch, J. Dalibard, W. Zwerger, *Rev. Mod. Phys.* **80**, 885 (2008)

134. D. Jaksch, C. Bruder, J.I. Cirac, C.W. Gardiner, P. Zoller, Phys. Rev. Lett. **81**, 3108 (1998)
135. A. Isacsson, M.C. Cha, K. Sengupta, S.M. Girvin, Phys. Rev. B **72**, 184507 (2005)
136. S.D. Huber, E. Altman, H.P. Büchler, G. Blatter, Phys. Rev. B **75**, 085106 (2007)
137. A. Micheli, G.K. Brennen, P. Zoller, Nature **2**, 341 (2006)
138. M.P.A. Fisher, P.B. Weichman, G. Grinstein, D.S. Fisher, Phys. Rev. B **40**, 546 (1989)
139. K. Byczuk, D. Vollhardt, Phys. Rev. B **77**, 235106 (2008)
140. A. Hubener, M. Snoek, W. Hofstetter, Phys. Rev. B **80**, 245109 (2009)
141. W.J. Hu, N.H. Tong, Phys. Rev. B **80**, 245110 (2009)
142. P. Anders, E. Gull, L. Pollet, M. Troyer, P. Werner, Phys. Rev. Lett. **105**, 096402 (2010)
143. K. Byczuk, D. Vollhardt, Ann. Phys. (Berlin) **18**, 622 (2009)
144. J. Dziarmaga, Adv. Phys. **59**, 1063 (2010)
145. A. Polkovnikov, K. Sengupta, A. Silva, M. Vengalattore, Rev. Mod. Phys. **83**, 863 (2011)
146. L. Perfetti, P.A. Loukakos, M. Lisowski, U. Bovensiepen, H. Berger, S. Biermann, P.S. Cornaglia, A. Georges, M. Wolf, Phys. Rev. Lett. **97**, 067402 (2006)
147. S. Wall, D. Brida, S.R. Clark, H.P. Ehrke, D. Jaksch, A. Ardavan, S. Bonora, H. Uemura, Y. Takahashi, T. Hasegawa, H. Okamoto, G. Cerullo, A. Cavalleri, Nature Physics **7**, 114 (2011)
148. P. Schmidt, H. Monien, arXiv:cond-mat/0202046
149. V. Turkowski, J.K. Freericks, Phys. Rev. B **71**, 085104 (2005)
150. R. van Leeuwen, N.E. Dahlen, G. Stefanucci, C.O. Almbladh, U. von Barth, in *Time-dependent density functional theory, Lecture Notes in Physics*, vol. 706, ed. by M.A.L. Marques, C.A. Ullrich, F. Nogueira, A. Rubio, K. Burke, E.K.U. Gross (Springer, Berlin, 2006)
151. M. Eckstein, M. Kollar, P. Werner, Phys. Rev. B **81**, 115131 (2010)
152. M. Eckstein, M. Kollar, P. Werner, Phys. Rev. Lett. **103**, 056403 (2009)
153. M. Eckstein, P. Werner, Phys. Rev. B **82**, 115115 (2010)
154. M. Eckstein, A. Hackl, S. Kehrein, M. Kollar, M. Moeckel, P. Werner, F.A. Wolf, Eur. Phys. J. Special Topics **180**, 217 (2010)
155. J.K. Freericks, H.R. Krishnamurthy, T. Pruschke, Phys. Rev. Lett. **102**, 136401 (2009)
156. M. Eckstein, M. Kollar, Phys. Rev. B **78**, 245113 (2008)
157. B. Moritz, T.P. Devereaux, J.K. Freericks, Phys. Rev. B **81**, 165112 (2010)
158. M. Eckstein, M. Kollar, Phys. Rev. B **78**, 205119 (2008)
159. J.K. Freericks, V.M. Turkowski, V. Zlatić, Phys. Rev. Lett. **97**, 266408 (2006)
160. M.T. Tran, Phys. Rev. B **78**, 125103 (2008)
161. J.K. Freericks, Phys. Rev. B **77**, 075109 (2008)
162. A.V. Joura, J.K. Freericks, T. Pruschke, Phys. Rev. Lett. **101**, 196401 (2008)
163. N. Tsuji, T. Oka, H. Aoki, Phys. Rev. B **78**, 235124 (2008)
164. N. Tsuji, T. Oka, H. Aoki, Phys. Rev. Lett. **103**, 047403 (2009)
165. M. Eckstein, T. Oka, P. Werner, Phys. Rev. Lett. **105**, 146404 (2010)
166. N. Tsuji, T. Oka, P. Werner, H. Aoki, Phys. Rev. Lett. **106**, 236401 (2011)
167. M. Eckstein, M. Kollar, Phys. Rev. Lett. **100**, 120404 (2008)
168. M. Eckstein, M. Kollar, New J. Phys. **12**, 055012 (2010)
169. N. Eurich, M. Eckstein, P. Werner, Phys. Rev. B **83**, 155122 (2011)
170. M. Rigol, V. Dunjko, M. Olshanii, Nature **452**, 854 (2008)
171. M. Moeckel, S. Kehrein, Phys. Rev. Lett. **100**, 175702 (2008)
172. M. Moeckel, S. Kehrein, Ann. Phys. **324**, 2146 (2009)
173. M. Greiner, O. Mandel, T.W. Hänsch, I. Bloch, Nature **419**, 51 (2002)
174. A. Rapp, G. Zarand, C. Honerkamp, W. Hofstetter, Phys. Rev. Lett. **98**, 160405 (2007)

175. M. Snoek, I. Titvinidze, C. Toke, K. Byczuk, W. Hofstetter, *New J. Phys.* **10**, 093008 (2008)
176. U. Schneider, L. Hackermüller, S. Will, T. Best, I. Bloch, T.A. Costi, R.W. Helmes, D. Rasch, A. Rosch, *Science* **322**, 1520 (2008)
177. J.K. Freericks, *Transport in multilayered nanostructures — The dynamical mean-field approach* (Imperial College Press, London, 2006)
178. M. Potthoff, W. Nolting, *Phys. Rev. B* **59**, 2549 (1999)
179. M. Takizawa, H. Wadati, K. Tanaka, M. Hashimoto, T. Yoshida, A. Fujimori, A. Chikamtsu, H. Kumigashira, M. Oshima, K. Shibuya, T. Mihara, T. Ohnishi, M. Lippmaa, M. Kawasaki, H. Koinuma, S. Okamoto, A.J. Millis, *Phys. Rev. Lett.* **97**, 057601 (2006)
180. L. Chen, J.K. Freericks, *Phys. Rev. B* **75**, 1251141 (2007)
181. K. Byczuk, in *Condensed Matter Physics in the Prime of the 21st Century: Phenomena, Materials, Ideas, Methods*, ed. by J. Jedrzejewski (World Scientific, Singapore, 2008), p. 1
182. R.W. Helmes, T.A. Costi, A. Rosch, *Phys. Rev. Lett.* **100**, 056403 (2008)